Raja Ramanna
Centre for Advanced Technology
Indore

Annual Progress Report: 2017-18

Raja Ramanna Centre for Advanced Technology, Indore

Annual Progress Report :2017-18

I. INDUS SYNCHROTRONS :

I.A. Indus accelerators Operation :

The synchrotron radiation sources, Indus-1 and Indus-2, are being operated in round-the-clock mode as a national facility. Indus-1 is operated at 450 MeV energy, 100 mA current, and Indus-2 is operated at 2.5 GeV energy and current upto 200 mA. The facility underwent a major upgrade in 2017. This entailed installation and commissioning of the first indigenously developed RF cavity in Indus-2, replacement of the microtron with an improved version and upgradation of transport line (TL-1) from microtron to booster synchrotron. During 2017, the Indus machines operated for 325 days. A larger amount of time (22 days) was provided for machine experiments this year. Despite this the beam availability to users was more than 6500 hours for Indus-1 and more than 5000 hours for Indus-2. Figures A.1 and A.2 depict the typical user mode operation of Indus-2 at 2.5 GeV energy. It may be noted that the average beam availability per day for Indus-2 has shown only a marginal increase this year, which is due to the fact that several short planned shutdowns had to be taken for the machine upgradation carried out throughout the year.

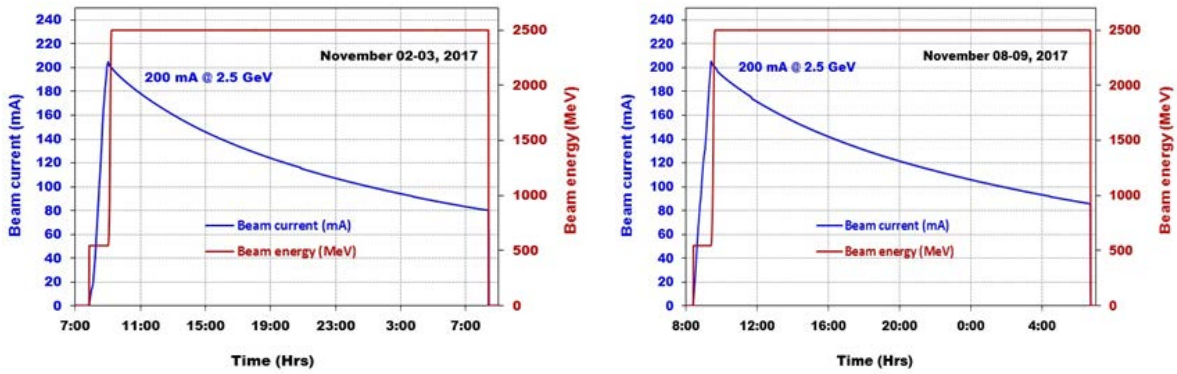

Fig. A.1 and 2 : Indus-2 operation with ~ 200 mA stored beam current at 2.5 GeV energy.

I.B. Upgradation of Indus-2 :

I.B.1. Installation, commissioning and deployment of indigenously developed RF cavity:

The first 505.8 MHz. bell shaped copper RF cavity, designed and developed indigenously, was assembled with input power coupler, higher order modes frequency shifter (HOMFS) and tuning system. The cavity was installed and commissioned in Indus-2 (Fig. I.B.1). Necessary modifications in the vacuum chamber were done to integrate the new RF cavity in the long straight section LS-7 of Indus-2. The RF cavity (Fig.I.B.2) integrated with high power solid state RF station through a 6-1/8 inch transmission line system.

With this indigenous RF cavity deployed along with the existing four other RF cavities, more than 200 mA beam current at 2.5 GeV beam energy was achieved in Indus-2. Two more such cavities will be developed and installed to provide the extra power required for operation of Indus-2 with insertion devices.

Fig. I.B.1: RF cavity installation in the Indus-2 ring straight chamber.

Fig.I.B.2: RF Cavity installed and connected to RF power station through transmission line .

I.B.2. Improvement in injector system of Indus Accelerators :

The aging 20 MeV/ 30 mA injector microtron of the Indus accelerators was replaced with a new upgraded version. (Fig I.B.2.1). The new microtron has improved mechanical design and additional diagnostic features for better performance. The Transport line-1(TL-1) which takes the microtron beam to the booster synchrotron, was also upgraded by installing new vacuum chambers, B-A gauges, upgraded beam position monitors and additional beam slit monitors (Fig I.B.2.2). Further, to improve the booster synchrotron operation, an electronic degaussing module has been developed and integrated with the microtron power supply to remove the remenant field of the dipole magnet and improve the repeatability of beam parameters of microtron.

Fig.I.B.2.1: New 20 MeV Injector microtron for Indus.

Fig.I.B.2.2: Modified Transport line-1.

I.B.3. Development and upgradation of the various power supplies for Indus accelerators:

Several types of specialized power converters and power supplies with improved performance were developed, installed, and commissioned in various sub-system of Indus-1 and Indus-2. Power converters include; two 300 A power converters for TL-2 dipole magnets, twenty card-

based power converters for 30 MeV injector linac, two units of 200 A, 85 V power converters to energize main coil of the harmonic sextupole magnet, and 200 A, 60 V power converter to energize solenoid coil for NEG coating. Power supplies include; capacitor charging power supply using series resonant topology for Indus-1 injection kicker, high voltage, high current and short pulse power supply for other applications. This has contributed significantly to the improvement in reliability of sub-systems due to which beam filling events have reduced.

I.B.4. Development of enhanced version of betatron tune feedback system for Indus-2:

A betatron tune feedback system is used in Indus-2 to ensure electron beam stability and to maintain the betatron tune constant within specified band during machine operation. An enhanced version of betatron tune feedback system has been developed and successfully tested in Indus-2. Block diagram of the system is shown in Fig.I.B.4. In the enhanced version, fast Fourier transform (FFT) of bunch-by-bunch beam position data, obtained from the Indus-2 bunch-by-bunch feedback system, has been used to determine betatron tune. Betatron tune in horizontal and vertical planes are measured simultaneously in the new scheme whereas in the existing scheme these are measured sequentially. The enhanced version performs ten times faster corrections of very small changes in the betatron tune (± 0.0005) which may occur due to changes in the machine optics. The system will be now provided to users on a regular basis.

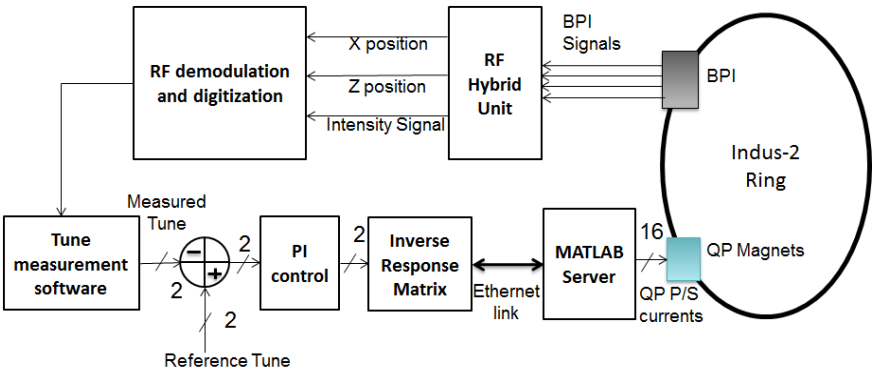

Fig.I.B.4: Block diagram of enhanced betatron tune feedback system.

I.B.5. Development of temperature sensor for hot spot detection:

During operation of Indus-2, due to change in power levels, the synchrotron radiation may hit the dipole magnet vacuum chamber which causes heating and degrades vacuum leading to degraded electron beam. It is of high interest to identify the hot spots and take appropriate measures to remove them. A Raman optical fiber distributed temperature sensor (ROFDTS) has been developed and deployed for detection of hot spot in one of the dipole magnet vacuum chambers (DP-2) of Indus-2 (Fig.I.B.5.1) A hot spot was detected 1.8 m from the entry point of electron beam and was arrested by correcting the beam orbit at that location. The measured temperature profile of DP-2 was also verified by reference thermocouples (Fig.I.B.5.2)

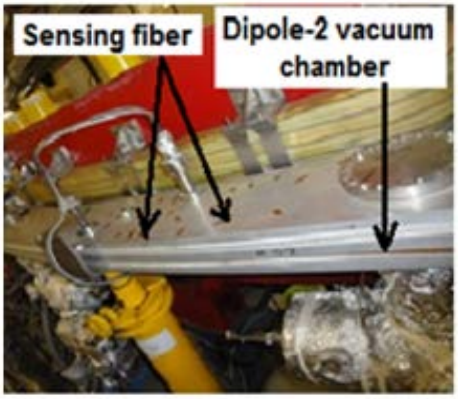

Fig.I.B.5.1: Hot spot detection in dipole measured magnet-2 of Indus-2.

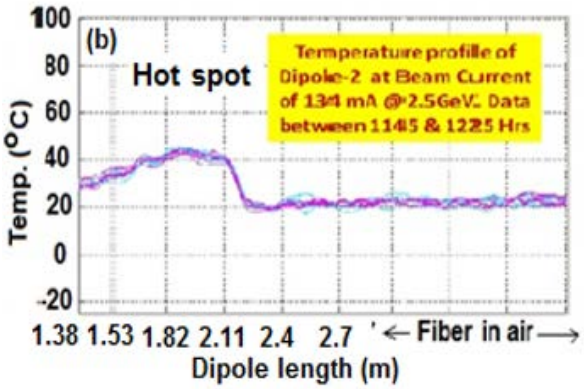

Fig.I.B.5.2: Temperature profile using ROFDTS .

I.B.6. Development of new control systems for the Indus facility :

Some additional control systems have been developed and deployed in the Indus synchrotron radiation source facility. These include: 1) A new control system with distributed architecture for remote monitoring and control of power supplies of magnets of the Transport Line-2, and Indus-1 storage ring, and 2) a control system for verification of correctness of cycling of the output current of magnet power supplies.

I.B.7. Developments and enhancements in web based Indus machine management software:

Various web based software packages have been developed or upgraded. These include: 1) *e-Logbook* for electronic logging and report generation of Indus operation, 2) *f-Logbook* for tracking the faults occurred in different subsystems during round the clock operations of Indus-1 and Indus-2, 3) *Indus-Online* for providing the live, historical, statistical and diagnostics data of Indus-1 and Indus-2 in tabular and graphical format over RRCAT-Intranet.

I.B.8. Development of upgraded subsystems for Indus facility: During 2017, upgraded versions of several subsystems of the Indus SRS facility have been developed and tested. These will be deployed in near future. Details of these subsystems are as follows:

I.B.8.1. Upgrade of pulsed injection kicker magnets of Indus Synchrotron Radiation Sources:

To facilitate the injection of the electron beam from the upcoming 30 MeV linac (in addition to the existing 20 MeV microtron), three new pulsed kicker magnets (Fig.I.B.8.1.1) with low coupling impedances have been developed for the booster synchrotron. These magnets have been developed using high frequency Ni-Zn-Co ferrite blocks with eddy current strip. A kicker with conductor windings around the ferrite along beam path showed a significant reduction of longitudinal coupling impedance without affecting kicker field pulse shape & its distribution. The up-graded injection kicker magnets with reduced longitudinal coupling impedance are shown in Fig.I.B.8.1. 2. These newer magnets will replace the existing lumped kicker magnets which will improve injection efficiency into 700 MeV booster synchrotron.

Fig.I.B.8.1.1: Upgraded pulsed injection kicker magnets.

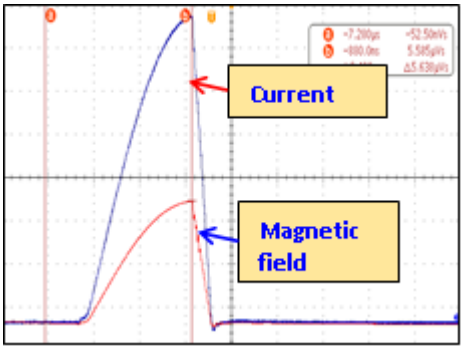

Fig.I.B.8.1.2: Up-graded injection kicker magnets with reduced longitudinal coupling

I.B.8.2. Modification in Indus-2 dipole magnet:

To extract the synchrotron radiation from 0° ports, the existing dipole magnet vacuum chamber (approx. 3.6 meter length) of Indus-2, was machined by increasing the slot height and width using in-house developed tools and fixtures (Fig I.B.8.2). Machining the slot in a in a closed chamber where the surface to be machined is not approachable or visible was a very challenging task. Special 1.5 m long hole milling cutters and tailor made fixtures were developed to guide the cutter during machining of slot on horizontal boring machine.

Fig.I.B.8.2: Indus-2 dipole magnet vacuum chamber after modifications.

I.B.8.3. Upgradation of beam diagnostic system of Indus-2 :

Beam scrapers are used in Indus-2 for measurement of dynamic aperture of electron beam. For example, these were used to decide the minimum physical aperture at undulator section. Existing scrapers have served for almost 10 years and are limited to 60 mA of beam current.

Upgraded beam scrapers (Fig.I.B.8.3.1 & Fig.I.B.8.3.2) have now been developed to allow their use at higher beam current of up to 200 mA at 2.5 GeV beam energy. This involved the development of vacuum joint between flange and cooling tubes with electrical isolation of the scraping blade, keeping thermal stresses within allowable limit. The assembly of scrapers has been qualified for ultra-high vacuum of ~4 X 10^{-10} mbar.

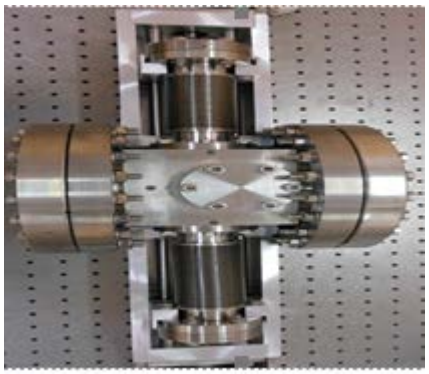

Fig. I.B.8.3.1: In-house developed upgraded horizontal scraper for Indus-2.

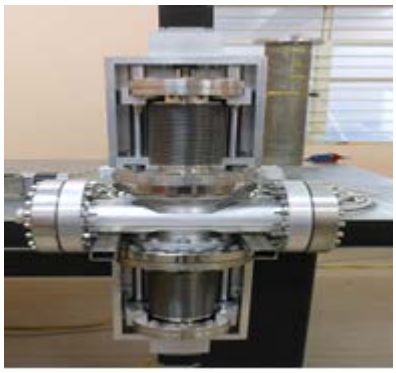

Fig. I.B.8.3.2: In-house developed upgraded vertical scraper for Indus-2.

Beam position monitor is a diagnostic device used for the measurement of the position of a charged particle beam. A UHV compatible flange integrated beam position monitors (FIBPM) has been indigenously designed and developed. In view of its small thickness, it can be installed in a limited space in an accelerator. Two versions of FIBPMs have been designed and developed. In one of the version (FIBPM-70OD) four numbers of button electrodes are integrated in 70 mm OD conflat flange whereas in another version (FIBPM-152OD) these are integrated in 152 mm OD diamond seal flange (Fig. 1). The button electrodes of FIBPM were welded by Nd:YAG laser (Fig. I.B.8.3.3).

Fig.I.B.8.3.3 : In-house developed ultra-high vacuum compatible FIBPM-152OD (left) and FIBPM-70OD (right).

I.B.8.4. Development of non-evaporable getter coated aluminium chamber for Indus-2 :

The aluminium chamber (17 mm x 81 mm and 300 mm) for Indus-2 was coated with a non-evaporable getter (NEG) coating using DC magnetron sputter deposition system. The challenge involved was the placement of target coaxially inside the chamber. Chamber was coated at 600V discharge voltage, 100mA discharge current, 1.5×10^{-3} mbar argon pressure, 400G magnetic field and at 100^{o}C substrate temperature. Before coating, the ultimate vacuum achieved in the system was 1.2×10^{-9} mbar. The NEG coated chamber was activated at 180 ^{o}C for 24 hrs and ultimate vacuum of 3×10^{-11} mbar was achieved.

I.B.8.5. Design and development of 505.8 MHz RF circulator:

A circulator is used for protecting as high power RF amplifiers from the reflected power when coupled to a RF Cavity. It works as a dynamic switch by forwarding the reflected power towards a dummy load. A high power, three port 505.8 MHz RF circulator has been designed, developed and tested. The circulator was tested at high power where return loss of better than 23 dB and insertion loss better than 0.1 dB with isolation of 25 dB for 60 kW input power was obtained. (Fig. I.B.8.5).

Fig. I.B.8.5: High power RF testing of 505.8 MHz circulator.

I.C. Indus beamlines utilization and up-gradation :

I.C.1. Utilisation of Indus beamlines :

Indus -1 and Indus-2 are national facilities with 10 beamlines in Indus-2 and 6 in Indus-1 available to users. More than 700 user experiments were carried out in the calendar year 2017 leading to 120 research publications in peer reviewed international journals. Some of the work carried out using the beamlines is briefly described below:

RRCAT in collaboration with Indian Space Research Organization / Indian Institute of Astro physics, has developed multilayers of tungsten / boron carbide (W/B_4C) for multilayer reflective mirrors (Fig. I.C.1.1) to be used in x-ray telescopes for astronomical applications. The performance of these mirrors have been evaluated in the energy range 9 keV to 16 keV using the BL-16 beamline of Indus-2, and measured reflectivity curves and are shown in Fig.I.C.1.2. The mirror reflectivity is found to be appropriate for fabrication of compact telescopes suitable for a space payload.

Fig. I.C.1.1: W/B_4C multilayer x-ray mirror developed at RRCAT

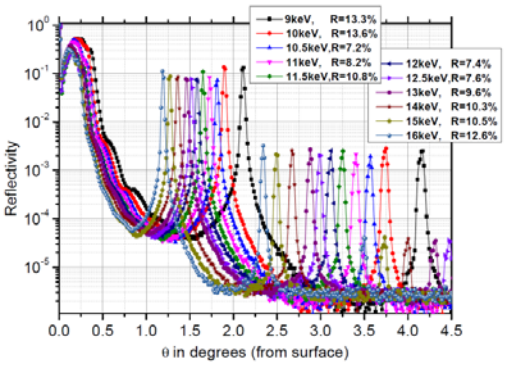

Fig.I.C.1.2. Measured XRR curves of W/B_4C ML(d = 1.88 nm and N =170) in the energy range 9 to 16 keV using BL-16, Indus-2.

Several users have utilized the Indus beamlines to study various materials of potential technological interest. Some examples are:

- Determination of crystal and electronic structure of NiO and Zn substituted NiO for applications to transparent electronics and antiferromagnetic spintronics: Pulsed laser deposition has been used for the growth epitaxial NiO layers on GaN substates. Epitaxial NiO layer is found to have two domain structures oriented along the [111] direction with an in-plane rotation of ~60^o with respect to each other. In another study on Zn substituted NiO, the variation of Ni-O and Zn-O bond length with percentage substitution has been determined using EXAFS measurements at BL-09, Indus-2. These studies have also given an insight to the mechanism of phase separation in Zn substituted NiO at ~ 30% Zn substitution.

- Determination of crystalline and electronic structure of cobalt based ferrites for memory devices: The electronic properties of $Co_{1.5}Fe_{1.5}O_4$ have been studied using oxygen K-edge and TM (Fe and Co) $L_{2,3}$ edge X-ray absorption at BL-01 Indus-2, whereas low temperature magnetic measurements show magneto-crystalline anisotropy with two clearly distinct pinning centers.

- Study of origin of efficient photoluminescence and high conductivity of metal interconnected graphene quantum dots (Fig.I.C.1.3) for solar cell applications: In this graphene based quantum dots connected by metal (Zn) and oxygen ions have been synthesized to understand the nature of the optical transition for the generation of blue light, observation of large photoconductivity and extremely low electrical resistance. X-ray absorption measurements carried out at BL-09 (in the hard x-ray region at the Zn edge), and BL-01(in the soft x-ray region at the Oxygen, and carbon edges) and quantum chemical calculations provide clear evidence for the metal-mediated growth process. The as-grown graphene quantum dot solids undergo a Resonance Energy Transfer interaction

thereby showing an extremely large 36% photoluminescence (PL) quantum yield in the blue region at 440 nm.

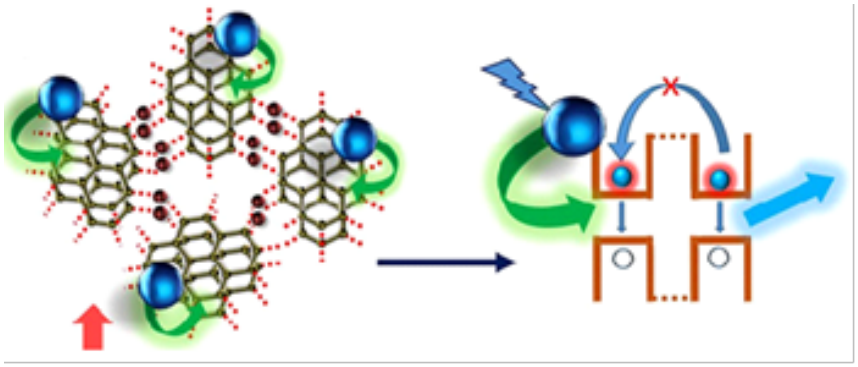

Fig. I.C.1.3: The structure of the metal atom based interconnected graphene quantum dots and the schematic of process of generation of high efficiency photoluminescence.

- Determination of electronic structure of semiconducting intermetallic alloy $FeGa_3$ for thermoelectric devices and study of negative thermal expansion of Ca_3FeAlO_5: Combined High pressure XRD and first principles density functional theory (DFT) based electronic structure calculations have been performed for $FeGa_3$ at ambient and high pressure to understand its electronic and structural properties. The equation of state of $FeGa_3$, obtained from the high pressure XRD measurements carried out at BL-11 Indus-2, show a good match with theoretical calculations.

- The protein crystallography beamline has been used for determination of the crystal structure of several proteins. Among them are: the human aminopeptidase XPNPEP3 (Fig.I.C.1.4) protein, which has a significant role in cystic kidney diseases; type III periplasmic proteins, (VcFhuD, VcHutB) (Fig.I.C.1.5), the knowledge of which will help in the development of treatments of certain types of drug resistant pathogen based diseases and Xaa-Pro dipeptidases (Fig.I.C.1.6) which are found in all living organisms and are believed to play an essential role in proline metaboli

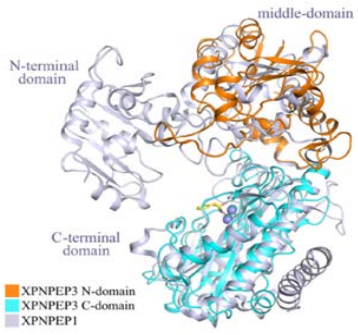

Fig.I.C.1.4: Structural superposition of XPNPEP3 and XPNPEP1 monomers.

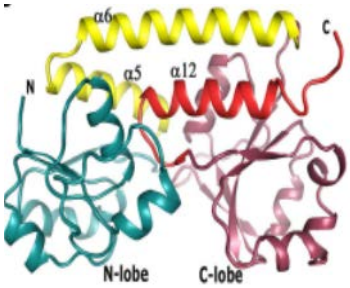

Fig.I.C.1.5: Structure of apo-VcFhuD.

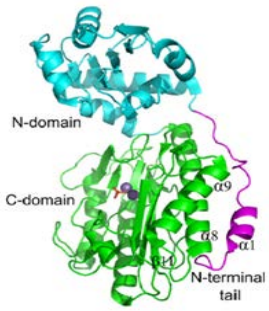

Fig.I.C.1.6: Domain organization and N-terminal interactions of XPDxc.

I.C.2. Upgradation of Indus beamlines :

Some of the Indus beamlines have been upgraded to carry out more challenging and novel experiments by the users. The main improvements are described below.

- The soft x-ray reflectivity beamline in Indus-1 has been upgraded by introducing the p-polarization measurement setup (Fig.I.C.2.1.). The p-polarisation geometry will be used for many research problems eg. the molecular orientation in complex organic thin film, application for plasmonic excitation study in soft x-ray/VUV region, and in our in-house multilayer research program for the development of polarization sensitive x-ray multilayer optics.

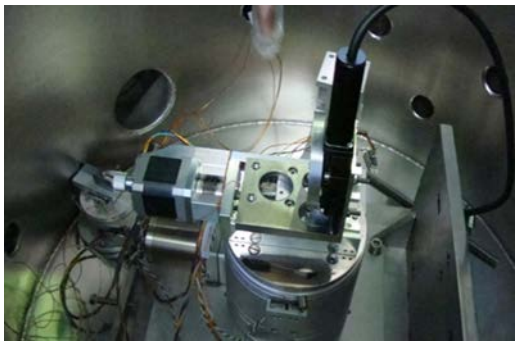

Fig.I.C.2.1: View of the p-polarisation setup at BL-04(Indus-1) beamline.

- The angle dispersive XRD beamline has been upgraded with the introduction of an evacuated flight tube at the detector side, to enable the measurement of diffraction patterns at low incident energies which will be specifically helpful in studies on the technological important 3D transition metals like iron, cobalt, nickel etc. (Fig. I.C.2.2.) shows the installed evacuated flight tube. The set up has been tested by performing grazing incidence XRD for Fe thin film (~30 nm thick) at 7 keV. We find no pattern without the flight tube because of absorption (in air) and scattering. The signal increases significantly after flight tube was integrated (Fig. I.C.2.3).

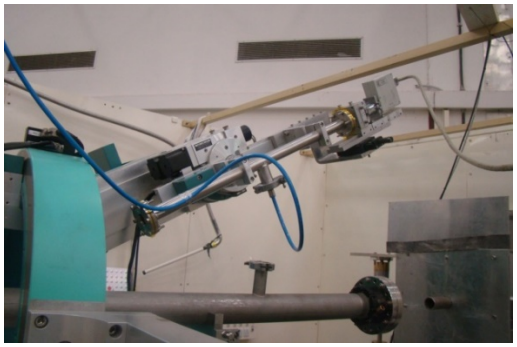

Fig.I.C.2.2. Photograph of the aligned flight tube on detector arm with evacuation arrangement

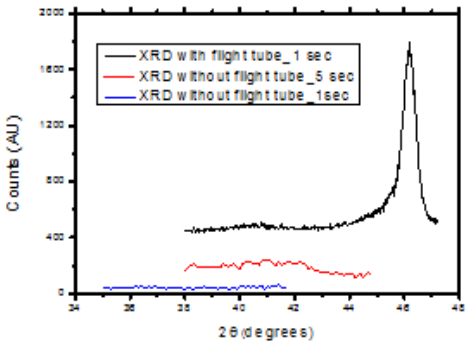

Fig.I.C.2.3. GIXRD pattern with and without Flight tube on Fe thin film. (~30 nm thick)

- After a decade of use, the toroidal mirror used in Indus-1 reflectivity beamline was severely contaminated with carbon deposits and the reflectivity had degraded. The mirror was cleaned using RF sputtering. This has enhanced the operation life of the toroidal mirror by more than a factor of two, thereby saving a large amount of expenditure (of the tune of ~ ₹ 20 Lakhs) for the import of a new mirror.

- Two frontends one for BL-05 and other for BL-10 beamline, have been designed, developed, commissioned and operated up to a beam current of 150 mA in Indus-2. These front-ends consists of specially designed water-cooled shutters, safety shutter, water-cooled mask and water-cooled beam viewer, capable of handling a heat load of 2.5 kW with very high thermal flux density. All the major components of both the front-ends are indigenously developed in RRCAT. Control system for remote operation of BL-10 beamline has been successfully developed.

II. ACCELERATOR TECHNOLOGY :

II.1. Development of a 650 MHz (β=0.92) five-cell Niobium SCRF cavity:

A prototype 650 MHz (β=0.92) five-cell superconducting radio frequency cavity has been fabricated (Fig. II.1). This is the first 5-cell, high beta, 650 MHz cavity fabricated in the country. The fabrication involved forming of high purity niobium sheet into half-cells, machining of the formed components, machining of end groups parts, and joining half-cells and end groups components using electron beam welding. Due to the very high Q, SCRF cavities are extremely sensitive to geometrical changes and due care is required at every stage of fabrication to control them. The SCRF cavity was subjected to various testing and qualification upon completion. The results are as given in Table 1.

Fig.II.1: First 650 MHz (β=0.92) five-cell SCRF cavity developed at RRCAT.

Parameter	Target	Achieved
Cavity Length(mm)	1400.25 ± 3	1403.942
π mode Frequency at 300 K (MHz)	649.592 ± 0.5	649.5922
Vacuum test leak rate (mbar.lit./sec)	$< 1 \times 10^{-11}$	$< 1 \times 10^{-11}$

Table.1: *Mechanical, RF and leak testing results.*

II.2. Indigenous development of a semi-automatic cavity tuning machine for tuning of five-cell 650 MHz SCRF cavities :

A semi-automatic cavity tuning machine for tuning of five-cell 650 MHz SCRF cavities has been designed and developed using the earlier experience of developing tuning machine for 1.3 GHz SCRF cavity (Fig.II.2.1). A five-cell 650 MHz SCRF cavity fabricated in niobium has been tuned using this machine. This development is based on the earlier experience in

developing a tuning machine for 1.3 GHz SCRF cavity. For an efficient acceleration of charged particle, it is required to have a uniform electric field in every cell of a multi-cell SCRF cavity. The cavity resonating frequency is also required to be matched with the RF supply frequency. The machine is designed and developed indigenously to achieve the required resonating frequency and field flatness (≥ 90 %) at room temperature. A software has been developed which calculates the necessary frequency corrections required for each cell of the cavity. By changing the resonating frequency of the cavity from 649.615 MHz to 649.264 MHz the field flatness was improved from 42% to 90.6% (Fig.II.2.2).

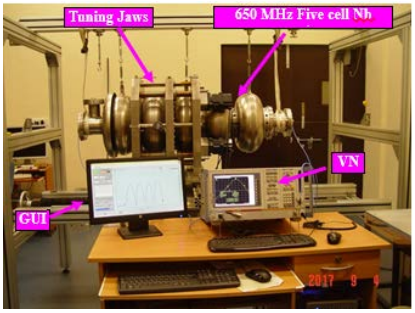

Fig. II.2.1: Indigenously developed semi-automatic cavity tuning machine for 650 MHz SCRF cavity.

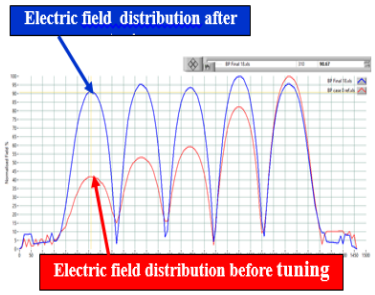

Fig. II.2.2: Normalised electric field distribution (before & after tuning).

II.3. Development of a computer code for study of multipacting in superconducting elliptic cavities :

Multipacting is one of the important performance limiting phenomena that is encountered while operating the superconducting radiofrequency (SRF) cavities at higher acceleration gradient. Computer simulations are essential to pre-empt this phenomenon, such that it can be avoided by refining the cavity shape suitably. A computer code has been developed and benchmarked for simulating the performance limiting phenomenon of multi-pacting in SCRF elliptic cavities (Fig II.3). This code takes less computational time and requires less computer memory compared to the currently used computer codes. In addition, a simplified model has also been worked out for the fast calculation of multipacting growth rates. Growth rate of multipacting is plotted (Fig.II.3) as a function of acceleration gradient for a TESLA 1.3 GHz elliptic cavity using (a) commercially available code (CST), (b) our code and (c) simplified model. The developed software is a good import substitute for the expensive commercial software.

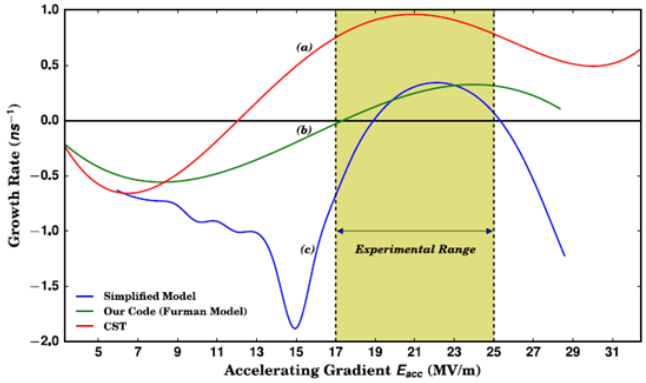

Fig. II.3: Indigenously developed computer code to study multipacting in superconducting elliptic cavities.

II.4. Development of modulators for high average power applications :

A 100 kV, 20 A, compact, all solid state long pulse converter modulator (Fig.II.4.1) and Marx modulator (Fig.II.4.3) to drive high average power klystrons for future linacs of Indian Spallation Neutron Source (ISNS) has been developed and tested at low pulse repetition rate on dummy resistive load.

The long pulse modulator consists of high frequency switched inverters (*fs=20 kHz*), high voltage high frequency transformer, fast six pulse rectifier and a filter. The inverters are based on PLR topology which inherently offers high voltage gain depending on the quality factor (Q). The 'phase shift control' method has been adopted for the primary inverter unit. The unique advantage of this scheme is high output ripple frequency of 120 kHz,that is six times of the basic switching frequency (20 kHz). For the converter modulator at 100 kV, a drop of ±1 % has been achieved (Fig.II.4.2).

The Marx modulator is composed of two units that are main Marx unit and corrector Marx unit. The main Marx unit generates 100 kV base pulse while corrector Marx unit compensates the droop of the base pulse by staggered triggering of its modules. For the Marx converter, the output drop at 100 kV was ±0.5 %.

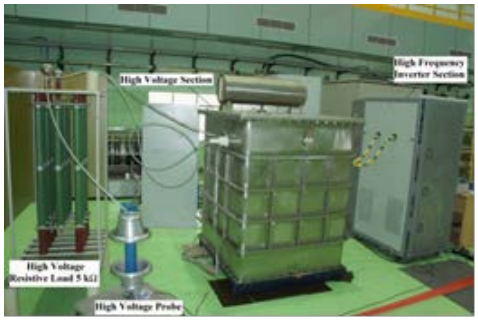

Fig II.4.1: Photograph of the modulator setup.

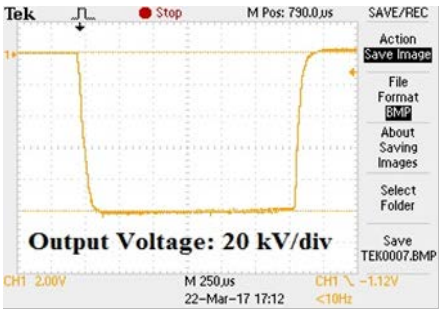

Fig.II.4.2: Modulator output voltage waveform at 100 kV.

Fig. II.4.3: Photograph of the Marx Modulator.

II.5. Development of brazed aluminium plate-fin heat exchanger for 50 lit/hr indigenous helium liquefier:

Compact brazed aluminium plate fin heat exchanger (Fig. II.5) have been developed through a local vendor for the operation of 50 lit/hr indigenous helium liquefier. A train consisting of six heat exchangers has been integrated in the helium liquefier and trial runs are in progress. This development will help in import substitution of medium size helium liquefiers.

Fig. II.5 : Brazed aluminum plate-fin heat exchanger

II.6. Indigenous concept for storage and transportation of fruits and vegetables using cryo-module technology:

A method has been conceptualized for storage and transportation of fruits and vegetables using liquid nitrogen (Fig. II.6). This system has been tested for the temperature between -50 ºC to 20 ºC. This system is expected to have an advantage of simple manufacturing process and low operating cost.

Fig. II.6: Table top version of the liquid nitrogen powered cold capsule for the reefer application.

II.7. Infrared free electron laser (IR-FEL) development :

An S-band, seven-cell (Fig.II.7.1), standing wave accelerating buncher has been designed, developed, tuned to the desired RF parameters with a field flatness < 3%, and qualified through low and high power testing. The buncher is designed to bunch a 90 keV electron beam to ~ 20 ps and to accelerate it to 1.5 MeV. An algorithm has been developed for the design and tuning of the buncher using minimal computing resources and with relaxed fabrication tolerances. The buncher has been successfully tuned using this algorithm to a resonant frequency of 2856 MHz with a field flatness < 3%. The field profile of the buncher before and after tuning is show in (Fig.II.7.2).

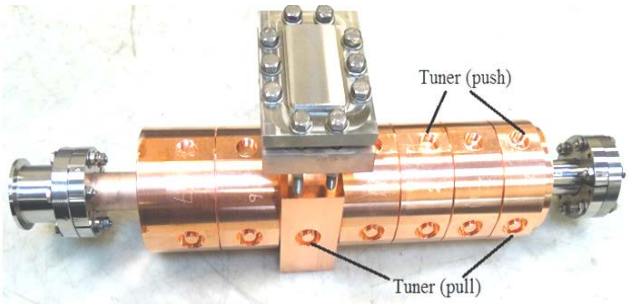

Fig. II.7.1: Picture of the seven-cell accelerating buncher.

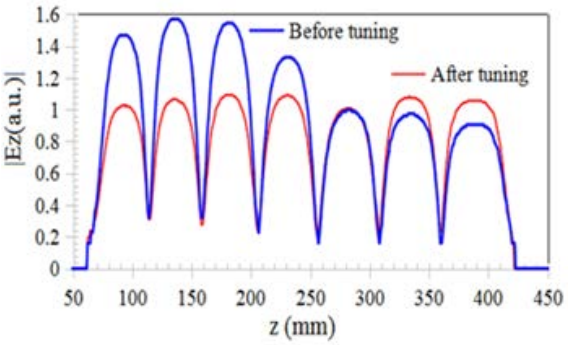

Fig. II.7.2: Field profile in the buncher before (blue) and after (red).

A solid state power amplifier has been developed for S-band pre-buncher of injector linac of infrared free electron laser (Fig II.7.3). The amplifier provides up to 2 kW of peak power at 2856 MHz ± 5 MHz with pulse width of 15 µs and repetition rate of up to 50 Hz. The amplifier has saturated gain of 9 dB.

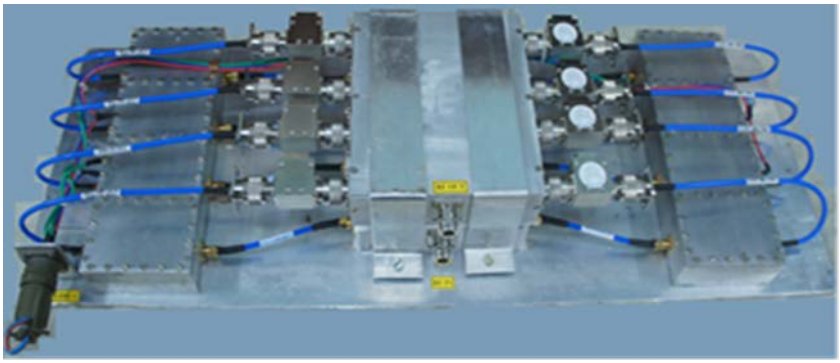

Fig. II.7.3: 2 kW solid state power amplifier for IRFEL injector LINAC's pre-buncher

II.8. Design and development of multi-cusp H^- ion source and high energy transport line for proton linac :

A filament arc discharge based multi-cusp H- ion source has been indigenously designed and developed to be used as an injector to the front end of H- Linac for SNS applications (Fig.II.8) to achieve the peak H^- ion beam current of 12 mA at accelerating voltage -50 kV DC with 100 amperes arc discharge current in pulsed mode. A high voltage ignitor electrode has been developed to create the background glow discharge hydrogen plasma inside the multicusp plasma. The H- ion beam was accelerated by floating the plasma chamber at -50 kV DC potential with respect to the ground electrode. The ion source was operated in pulsed arc mode with 2 Hz repetition rate and 0.5 ms pulse duration and extracted using 3-electrode extraction system The control system for remote operation was developed and deployed.

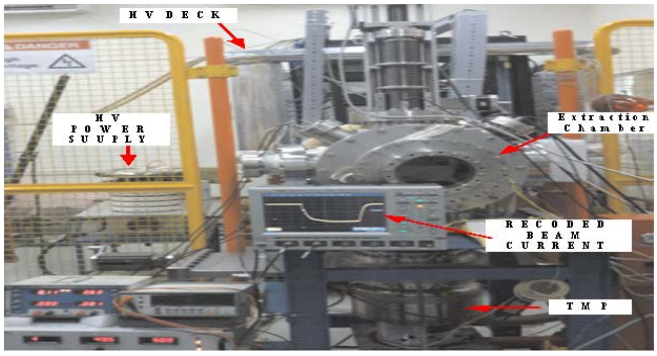

Fig. II.8: Front view of indigenously developed filament arc discharge multi-cusp H^- ion source for Proton Linac.

A high energy beam transport (HEBT) line has been designed to transport and match the 1 GeV, 1 MW H^- beam from the exit of the injector linac, up to the injection point of the accumulator ring, ensuring that the uncontrolled beam loss is within 1 nA/m, such that hands-on maintenance of the accelerator will be possible.

II.9. Development of magnets for mass spectrometers :

RRCAT has designed and developed nearly ten numbers of various dipole magnets with different bending radius and field value. These magnets are supplied to Technical Physics Division, BARC for manufacturing of mass spectrometers. Recently developed 0.8 tesla dipole magnet with 200 mm bending radius (Fig.II.9.1) supplied to BARC produced a radial magnetic field uniformity of 3×10^{-4}. The measured magnetic field uniformity ($\Delta B/B_0$) using Hall probe in radial direction at 0.3 T, 0.5 T and 0.8 T fields is shown in Fig. II. 9.2.

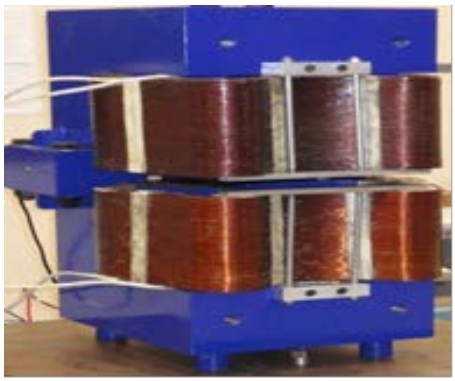

Fig. II.9.1: 200-R Mass-analyser dipole magnet

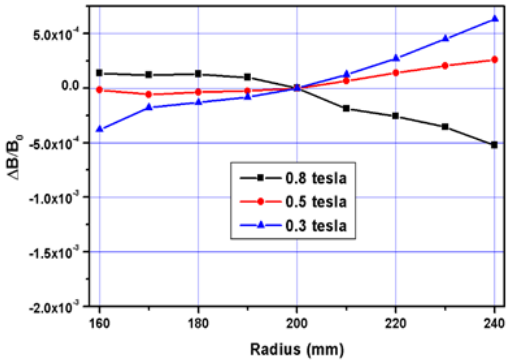

Fig. II.9.2: Measured field uniformity in dipole magnet.

II.10. Indigenous development of rotating coil based magnetic measurement system :

A rotating coil based measurement system (Fig.II.10) has been developed for the characterization of quadrupole and sextupole magnets. The measurement setup comprises of a rotating coil assembly of seven radial coils, a dc motor to rotate the coil assembly connected with an incremental encoder at the other end and a digital integrator for flux measurement. The results of the magnetic measurement in this system are found in agreement with those obtained with imported one. The reproducibility of the measured data is to be found within 1×10^{-4}. Fast

corrector magnets (40 Nos), combined function quadrupoles and new sextupole magnets have been characterized with this bench and successfully installed in the Indus-2 ring for fast orbit correction of electrons.

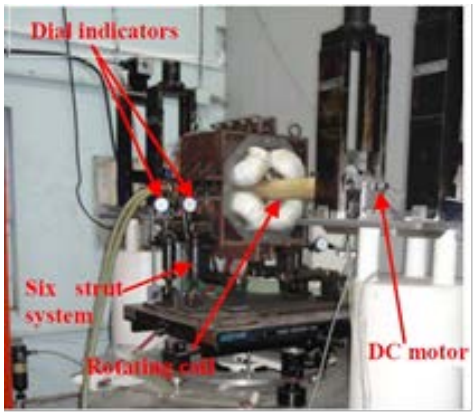

Fig. II.10: Indigenously developed Rotating coil based magnet measurement system.

II.11. Development of microcontroller based inverted magnetron gauge controller :

A microcontroller based inverted magnetron gauge controller and switch-mode power supply (SMPS) have been designed and developed indigenously. The SMPS is rated for 3.3 kV, 100 µA to power the gauge head. The controller has been tested to measure pressures in the range from 10^{-5} to 5 x 10^{-11} mbar. This is an import substitute and will be deployed in calibration of gauges.

II.12. Development of subsystems for the Agricultural radiation processing facility (ARPF):

One 10 MeV linac for irradiation of agricultural products has been already installed at the ARPF site near DABH fruit & vegetable mandi, Indore. The second linac to go here is under final testing. The accelerating structure for third 10 MeV electron linac has been fabricated. All major components of this linac were precisely machined and vacuum brazed (Fig. II.12.1). The accelerating structure was leak tested for the leak rate of < 10-10 mbar lit/s. The microwave system and electron gun for this linac have been developed. One similar system has been installed at the ARPF site (Fig. II.12.2).

Fig. II.12.1: Vacuum brazing of complete 10 MeV structure.

Fig. II.12.2: 6.0 MW microwave system and electron gun installed at ARPF site.

A beam profile measurement system has been developed and deployed for characterization of electron beam of industrial linacs developed at RRCAT. The system consists of two movable slit blades, one in horizontal and one in vertical direction, which scan the beam transversely. The slit blade is moved across the beam and current signal proportional to the portion of the beam falling on it versus blade position is measured. The accuracy of positioning of slit blades is better than 100 µm. The control electronics and the software developed for this system calculates and displays the beam parameters such as beam size, beam profile and beam position. The block diagram for the developed control and processing electronics of beam position monitor is shown in Fig.II.12.3.

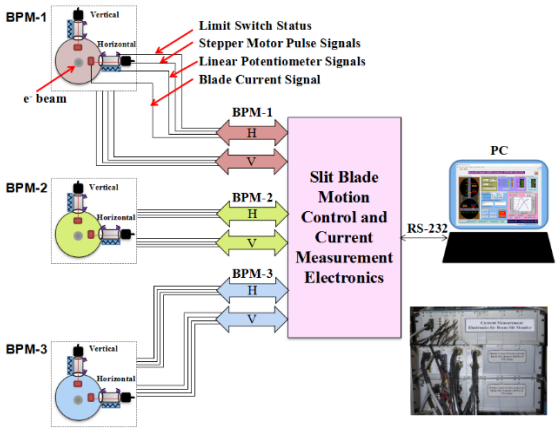

Fig.II.12.3: Block diagram of beam profile measurement electronics

II.13. Electron beam irradiation of various samples for agricultural and materials research:

This year irradiation experiments on agricultural products with the electron beam facility were carried out for several users. These included several varieties of rice, ground nut and tuberose bulbs (Fig. II.13.1,2,3). These were irradiated in a wide dose range from 20 Gy to 500 kGy using 10 MeV electron linac. Further, bio-fertilizer samples, medicinal samples, medical samples, jute fabric and semiconductor materials were electron beam irradiated for various end use application experiments.

a. Agricultural samples:

- Electron beam based mutation experiments of various varieties of rice, wheat, pulses and legume in the dose range of 150-300 Grey were taken-up in collaboration with Nuclear Agriculture & Biotechnology Division, BARC, Mumbai; Indira Gandhi Krishi Vishwavidyalaya (IGKV), Raipur and Chhattisgarh Engineering College, Durg (CG).
- Tuberose bulbs, an ornamental crop (*Arka sugandhi*, *Maxican single*), has been irradiated for mutation breeding studies at a dose range of 20 – 30 Gy (Fig. 3) in collaboration with ICAR-Indian Institute of Horticulture Research, Bangalore.

- The E-beam irradiation experiments conducted earlier for mutation breeding of ground nut (*Arachis hypogaea L.*) TG-26 variety has shown higher pod yield. The mutant is found to be stable after sixth generation.
- Postharvest manipulation of soybean with electron beam resulted in reduction of Anti Nutritional Factors (Trypsin inhibitor) and improving IVPD (*In-vitro* protein digestibility) in soybean seeds as well as in soy floor.

b. Bio-fertilizer samples

High molecular weight alginate and chitosan samples from Rashtrasant Tukadoji Maharaj (RTM) Nagpur University, Nagpur have been irradiated at a dose of 500, 600 & 700 kGy for its degradation in low-molecular weight forms which makes them water-soluble and can be used as bio-fertilizer plant growth stimulator, yield enhancer, fungicidal and biotic elicitor to enhance plant defense response against diseases.

c. Medicinal and medical samples

Ayurvedic medicinal plants (*T. terrestris, D. gangeticum, P. viscida*) from Kannur University, Kannur, Kerala have been irradiated to study the effect of irradiation on active components and shelf life at 5, 10 & 15 kGy dose.

d. Medical samples

Sialic acid samples from Shree Dhanvantary Pharmacy College, Kim, Surat were irradiated for induced grafting of Sialic acid on poly-capro lactones at 20, 40 & 60 kGy dose to be used for biocompatible encapsulation of therapeutic agents.

e. Jute fabric irradiation

Electron beam irradiaton of jute fabric has been carried out to study interfacial adhesion with thermosetting polymers to improve the surface roughness of jute fabric at 10, 100 & 250 kGy dose. The study is being carried out in collaboration with ICAR-National Institute of Research on Jute and Allied Fibre Technology, Kolkata.

f. Semiconductor materials

Semiconductor materials PHPL, PHL, PHP, PEO, PH, PZn, PTi, PL-10, PP, PLC, DE/Vp powder & ZnO, TiO_2 were irradiation using 8 MeV electrons to study the effect on physio-chemical properties at a dose of 40, 80, 120 kGy. This study is being carried-out in collaboration with University of Mangalore, Karnataka.

Fig13.1.1.Electron beam irradiation of rice seeds.

Fig.13.1.2.Electron beam irradiation of tuberose bulbs.

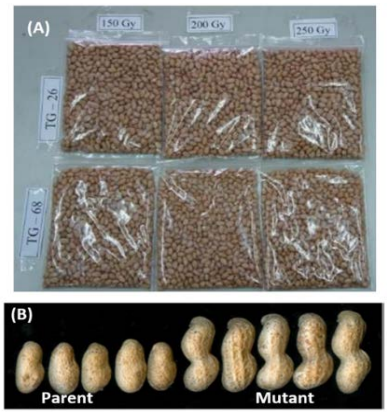

Fig.13.1.3 (A)E-beam Irradiated Ground nut TG 26 (B) Parent and mutant large pod size in M6 generation.

III. LASER TECHNOLOGY

The following lasers and laser based systems have been developed for industrial applications, nuclear applications and applied R&D:

III.1. Development and delivery of fiber coupled pulsed Nd:YAG laser system to IGCAR :

Two numbers of fiber coupled Nd:YAG laser systems capable of delivering 500 W average power and 10 kW peak power with pulse duration of 2-20 ms and pulse frequency in the range of 1-100 Hz have been developed and delivered to IGCAR for laser cutting of irradiated fuel subassemblies. (Fig.III.1.1). An electrical to optical conversion efficiency of 5.3% has been achieved. Beam quality of these lasers have been improved to a value of M^2 ~54 as compared to earlier value of ~83 by using the smaller diameter Nd:YAG laser rod. Laser cutting of up to 25 mm thick SS tubes has been demonstrated using these lasers (Fig.III.1.2).

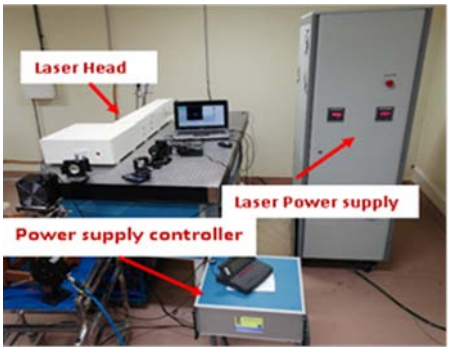

Fig. III.1.1 Schematic of 500 W Nd:YAG laser.

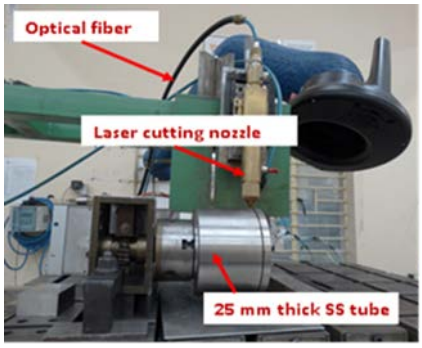

Fig. III.1.2. Shows a view of laser cutting mock-up of 25 mm thick SS.

III.2. Development of Nd:YAG laser system for laser welding of brachytherapy sources :

A compact Nd:YAG laser system with single lamp ceramic reflector pump chamber has been developed (Fig. III.2). This laser is capable of giving maximum energy of 12 J and the laser

pulse duration is 10 ms. The laser system is developed for Radiopharmaceutical Division, BARC and will be used for leak tight welding of radioactive iodine sources for brachytherapy treatment of eye and prostate cancer. The earlier system was made for BRIT, Mumbai which was used for welding of radioactive Iridium sources.

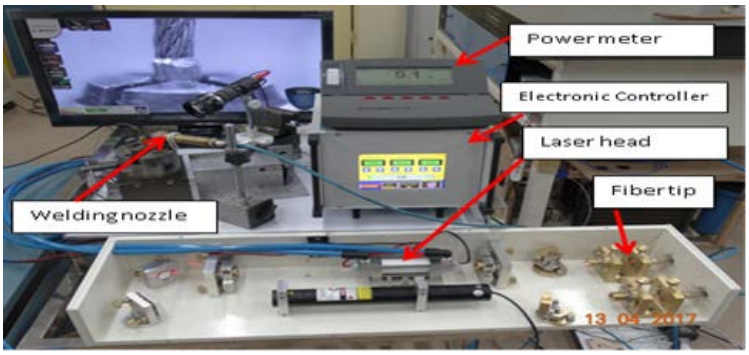

Fig. III.2: shows a view of in-house developed laser welding system for brachytherapy assemblies.

III.3. Development of all fiber laser:

III.3.1. An all-fiber Er-doped CW fiber laser capable of delivering 25 W at 1600 nm and line width of ~ 1.5 nm has been developed (Fig. III.3.1). In this development, commonly available pump diodes at 976 nm wavelength have been utilized instead of normally used costly 1480 nm pump diodes. Heat from Er-doped fiber is removed by coiling it on a water cooled spool. This laser has potential applications in remote sensing, range finding, skin surgery, and free space communication.

III.3.2. The output power of the earlier developed thulium-doped all-fiber CW laser was doubled by multiport pumping and with improved heat sinking of fiber components. The laser is now capable of delivering power of 34 W (Fig. III.3.2.). The optical-to-optical conversion efficiency observed is ~50%. The laser output is emitted from a fiber core of 12 μm and has single transverse mode. The laser output at 1940 nm has FWHM line width of ~0.1 nm, which is in eye-safe region. This laser has potential applications in plastic welding and micro surgery.

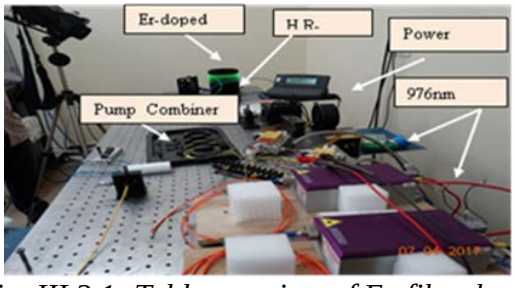

Fig. III.3.1: Table-top view of Er-fiber laser.

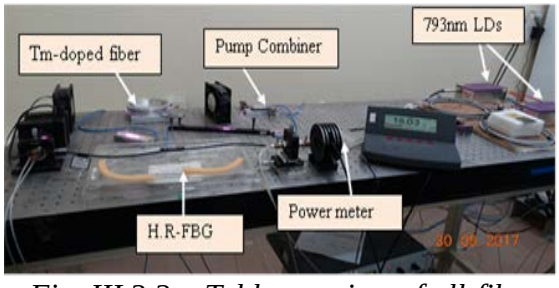

Fig. III.3.2: Table top view of all-fiber thulium-doped CW fiber laser.

III.3.3. Output power of earlier developed 400 W CW Yb-doped CW fiber laser was enhanced to about 500 W (Fig.III.3.3). This is due to improvement in development of low loss of 10

splice joints of different fiber components, heat management of splice joints along with control on self-pulsing. The optical-to-optical conversion efficiency observed is ~76% with a beam quality factor (M^2) of ~1.04. The laser output at 1080 nm has FWHM line width of ~0.6 nm. 500 W CW fiber laser will be useful in laser cutting of up to 6 mm thick SS and welding of up to 3 mm depth in SS.

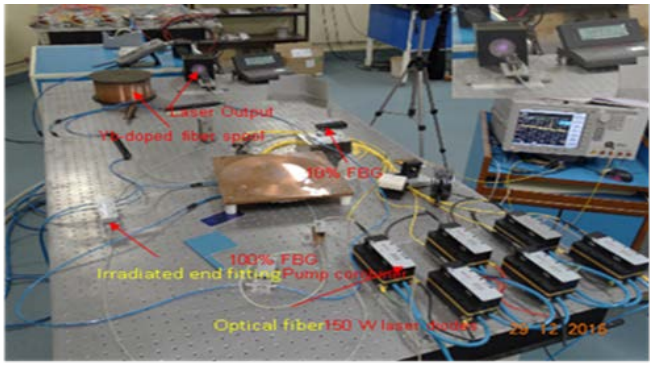

Fig. III.3.3: A view of in-house developed 500 W CW fiber laser.

III.3.4. An all fiber ultrafast oscillator-amplifier system shown in Fig III.3.4 at ~1070 nm wavelength has been developed. The output from the oscillator is amplified in multistages. The mode locked pulses are first stretched and then amplified in pre-amplifier stages. This laser system produces 42W of average amplified power at 40 MHz repetition rate. The pulses from the amplifier are highly chirped with ~70 ps duration which can be compressed to ~250 fs duration in an external grating-pair arrangement. This laser has potential applications in micro-machining.

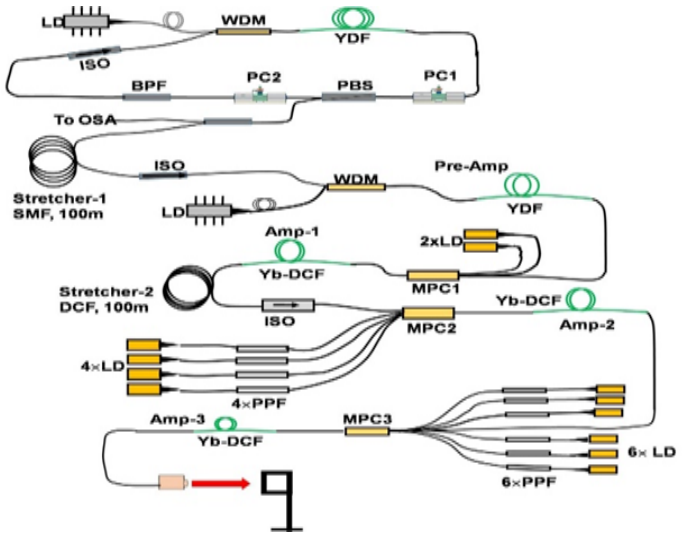

Fig. III.3.4 Schematic of all-fiber ultrafast oscillator-amplifier.

III.4. Development of 260 W average power at 532 nm :

A lab model of intra-cavity frequency doubled acousto-optic Q-switched Nd:YAG laser has been developed (Fig. III.4). The laser is capable of generating 260 W average power at 532 nm laser wavelength at 18 kHz repetition rate. The laser is designed in a thermal birefringence

compensated linear resonator having two pump heads, each having 30 number of laser diodes for transverse pumping of Nd:YAG laser rod in fivefold symmetry. The pulse duration (FWHM) was ~ 73 ns and optical to optical conversion efficiency is 16.8%. The beam pointing stability was measured to be ±2.8 micro rad. This laser has a potential for material processing of high reflectivity materials and pumping of tunable lasers such as dye laser, Ti sapphire laser etc.

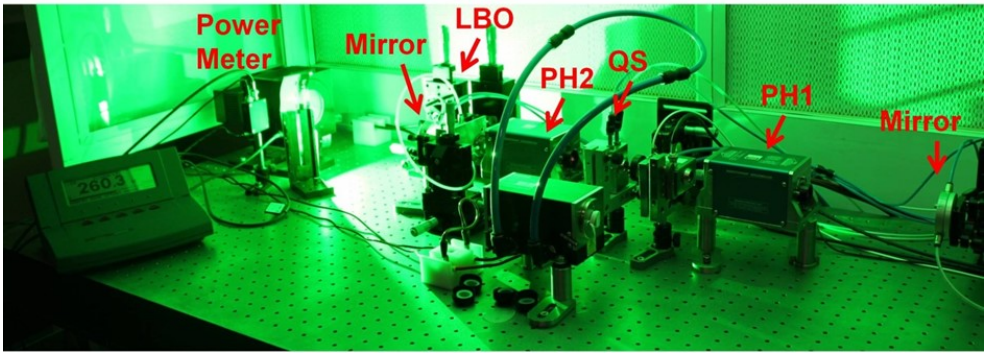

Fig. III.4: 260W diode pumped solid state green laser under operation.

III.5. Development of engineered model of diode pumped solid state (DPSS) green lasers at 6.25 kHz and at 9 kHz :

Last year two numbers of engineered version of diode-pumped solid state (DPSS) green laser systems were developed and installed at Hall-6, BARC for pumping of dye laser amplifier chain. This year two more numbers of engineered models of DPSS green lasers capable of delivering average output power of ~ 45 W at 532 nm and repetition rate of 6.25 kHz have been indigenously developed for BARC (Fig. III.5). The pulse duration of the laser measured was less than 40 ns (FWHM). Further, an experimental bench top model of DPSS green laser in coupled cavity configuration is also developed generating ~50W of average power with ~45 ns repetition rate at 9 kHz to meet the further requirement from BARC.

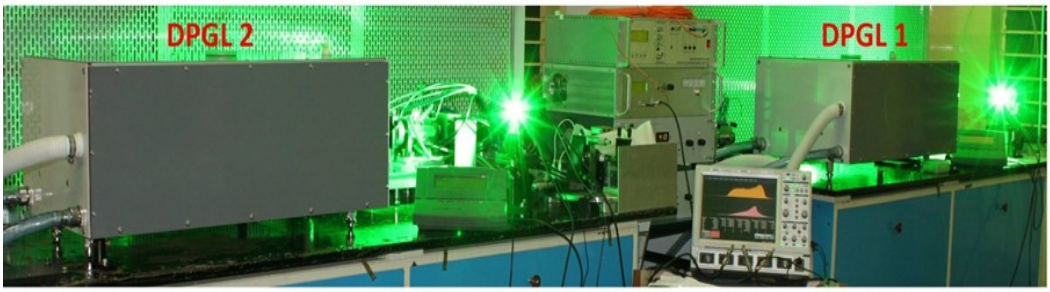

Fig. III.5: Two engineered diode pumped green lasers (DPGL1 and DPGL2) under operation.

III.6. Development of diode pumped fiber coupled high power CW Nd:YAG laser: A multi pump module, diode-pumped fibre coupled high power CW Nd:YAG laser (Fig. III.6) was developed. An overall output power of 1.92 kW at an optical to optical efficiency of 35% and M^2 value of 105 was achieved. The fibre coupling efficiency was 90%. This laser has potential applications in material processing namely sheet metal cutting, welding and cladding.

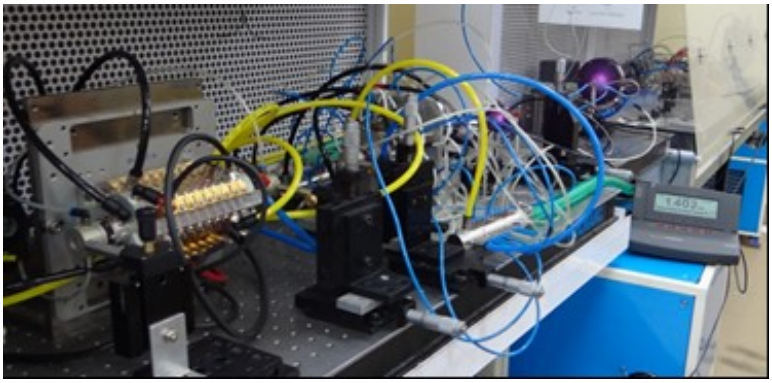

Fig. III.6: Diode pumped fiber coupled high power CW Nd:YAG laser.

III.7. Development of various power supplies, trigger generator for lasers and its applications:

Several Power supplies has been developed for the lasers and its applications. These includes: A 240 J, 5 Hz, simmer mode flash lamp power supply to drive a pair of xenon flash lamps in laser oscillator for laser shock peening applications, 15 kV - 20 kV, rise time < 100 ns, low timing jitter ± 4 ns, operating at 6.5 kHz power supply for copper vapor laser, 40 kV, < 200 ns rise time, at repetition rate of 0.2 Hz for triggering spark gap used for capillary discharge.

IV. LASER APPLICATIONS :

IV.1. Laser cutting of bellow lip weld joints of KAPS-2 reactor :

During en-masse coolant channel replacement (EMCCR) campaign at Kakrapara Atomic Power Station-2 reactor, laser cutting of 603 bellow lip weld joints (9 bellow lips already cut during single coolant channel removal operations) was carried out successfully using the earlier developed laser cutting procedure (Fig.IV.1.1 &1.2). Laser based cutting resulted in enormous reduction in MANREM consumption, time and cost.

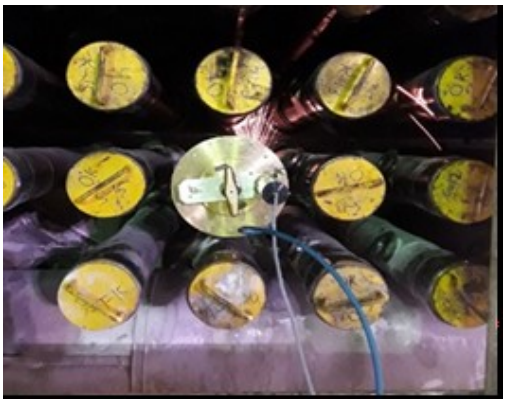

Fig. IV.1.1: In-situ laser cutting of bellow lip weld joints at KAPS-2 reactor.

Fig. IV.1.2: A view of separated bellow lips.

IV.2. Underwater laser cutting of pressure tube stubs of coolant channels of KAPS-2 reactor:

Underwater laser cutting of pressure tube stubs of 11 No. of coolant channels was carried out successfully after en-masse coolant channel replacement of KAPS-2 reactor (Fig. IV.2). Laser cutting of pressure tube stubs from each coolant channel was carried out in four circumferential

pieces which took ~4 hrs of laser operation. The post irradiation examination of pressure tube stubs near rolled joint area of pressure tube with end fittings was required to generate data on stresses and corrosion to improve the design of future PHWRs. All the pressure tube has to been transported to BARC for post irradiation studies.

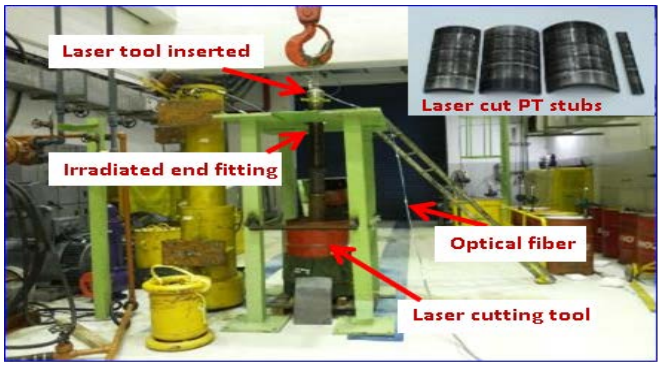

Fig. IV.2: Underwater laser cutting of pressure tube stubs in highly radioactive environment.

IV.3. Laser cutting technology for removal of Q-15 and P-18 coolant channels from KAPS-1 reactor :

Laser cutting technology was deployed for removal of Q-15 and P-18 coolant channels of KAPS-1 reactor (Fig.IV.3). For Q-15 coolant channel, end fitting having thickness of 18 mm was cut remotely near the rolled joint area in lead shielding flask and pressure tube stubs of P-18 coolant channel were cut underwater for post irradiation examination data. This resulted in minimum radiation dose consumption and in a very short time span without any airborne activity or radiation hazard.

Fig. IV.3: Laser cutting of 18 mm thick end fitting in lead shielding flask.

IV.4. Laser cutting of secondary shutdown system pipeline for replacement of double check valve at Kudankulam Nuclear Power Plant-1 reactor :

An *in situ* laser cutting system, using a compact tool with laser cutting nozzle and indigenously developed 250 W Nd:YAG laser, developed at RRCAT, was deployed for remote laser cutting of double check valve pipelines at four different locations of KKNPP-1 reactor at Kudankulam (Fig. IV.4). Implementation of remote laser cutting technique has resulted in sizable reduction in cutting time, radiation dose consumption by the personnel, and lesser secondary waste generation as compared to conventional mechanical methods.

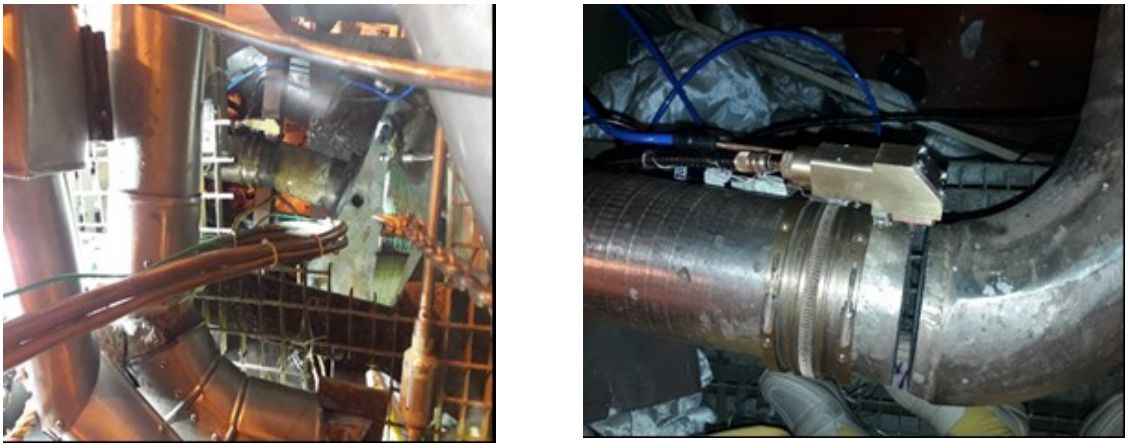

Fig. IV.4 :Remote laser cutting of double check valve pipelines at four different locations of KKNPP-1 reactor at Kudankulam.

IV.5. Laser cutting of triangular bocks at RAPS-3 reactor for enhancement of creep margin:

In-situ laser cutting of 18 number of 18 mm thick triangular blocks along with 1 mm thick washer (total 19 mm) was carried out successfully at Rajasthan Atomic Power Station-3 reactor with less radiation dose consumption (Fig.IV.5.1 & 5.2). This resulted in enhancement of creep margin of nine coolant channels by 19 mm and thereby enhanced operating life of power generation of these coolant channels by nine more years.

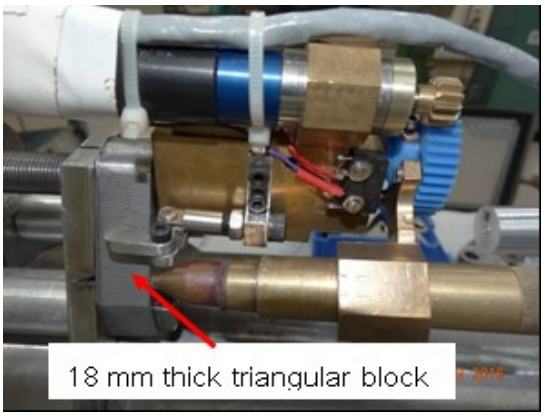

Fig. IV.5.1: Laser cutting fixture for triangular blocks.

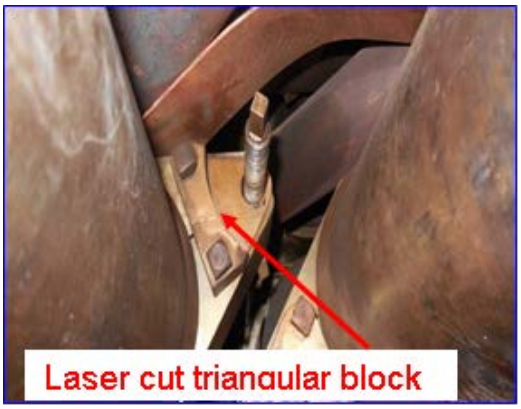

Fig. IV.5.2: Laser cut triangular block.

IV.6. Laser additive manufacturing of Deloro-50 bushes:

The bushes of the transfer arm of the gripper sub-assembly of the fast breeder reactor have to be wear and corrosion resistant at high temperature. These can be met using nickel based alloys, like – Colmonoy-6, Deloro-50 etc. RRCAT has successfully developed a technology for the fabrication of these Deloro-50 bushes (OD 18 mm, ID 15 mm, and 20 mm length) using laser additive manufacturing technique. The bushes of Deloro-50 have been fabricated using 2 kW fiber laser with substrate at preheating temperature of 400 ºC (Fig. IV.6). The LAM fabricated process has resulted in reduction in material wastage and machining of hard materials. Four such bushes were sent to IGCAR for field testing.

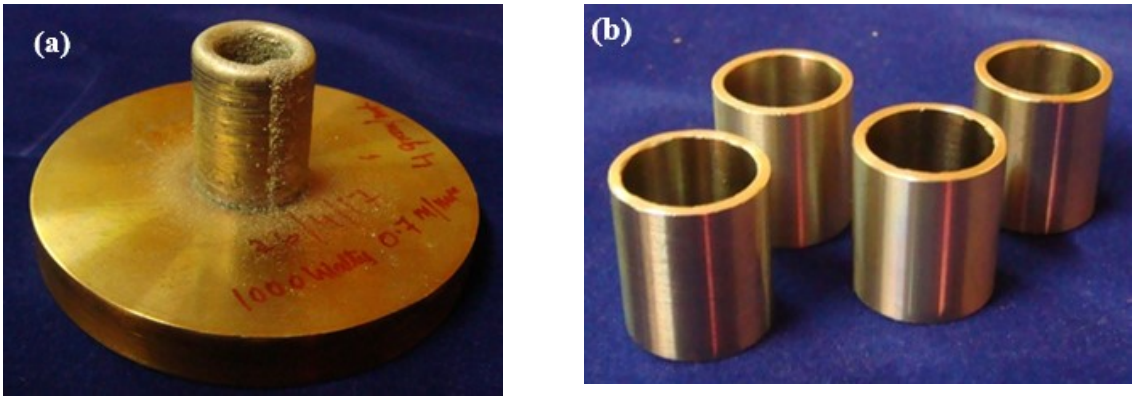

Fig.IV.6 Laser additive manufactured built Deloro-50 bushes (a) as-built and (b) post-machining.

IV.7. Installation of radioactive environment compatible fiber Bragg grating based temperature sensor system at BARC, Tarapur :

A fiber Bragg grating based temperature sensor system developed at RRCAT (Fig. IV.7), has been installed at the radioactive waste storage vault facility at Solid Storage Surveillance Facility, Nuclear Radiation Board, BARC, Tarapur. The system is being used for round the clock monitoring of temperature (40 - 50 ºC, with accuracy of ±1%) in the high radiation environment (dose rate ~7000 to 8000 rad/hr) storage vault located about 3 meter below the ground level.

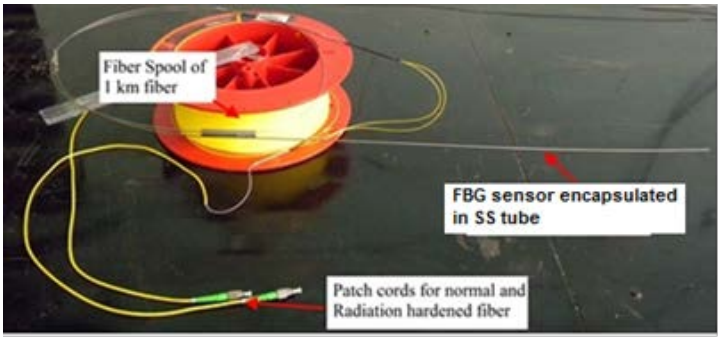

Fig. IV.7: Schematic of fiber Bragg grating sensor

IV.8. Laser shock peening for inter-granular corrosion suppression of sensitized 304 stainless steel (SS) and enhancing the fatigue life of hard chrome plated 15 - 5 PH SS:

Inter-granular corrosion (IGC) is responsible for failures of many austenitic stainless steel (SS) components operating in corrosive environment. It is due to microstructural degradation arise from inter-granular precipitation of Cr-rich carbides and development of chromium-depleted regions when exposed to temperatures of 500 - 800 ºC during welding. Significant suppression of inter-granular corrosion (IGC) susceptibility of sensitized 304 SS was achieved through laser shock peening(LSP) treatment using an in-house developed Nd-YAG laser (Fig. IV.8).

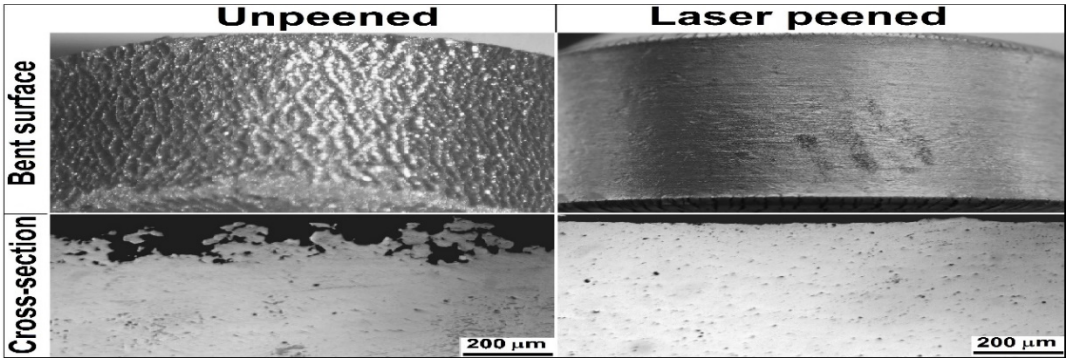

Fig. IV.8: Magnified views of bent surfaces (convex) and cross-sections of unpeened and triple laser peened specimens of sensitized 304 SS after ASTM A 262 practice E test.

Hard chrome plating used for enhanced wear and corrosion resistance suffers from loss of fatigue strength, due to presence of high tensile residual stresses and micro cracks. LSP has been exploited as a surface pre-treatment for effecting about 47% increase in fatigue life of hard chrome plated 15-5 PH stainless steel specimens.

IV.9. Development of a computer based cancer diagnostic system for screening of oral or cervical cancer:

A compact and portable computer based optical spectroscopic system (Fig. IV.9.1) was developed for screening of oral or cervical cancer. The system consists of a UV LED (for inducing fluorescence), a broadband white LED (for exciting diffuse-reflectance) and a chip-based miniaturized fiber-optic spectrometer, all accommodated in a rectangular housing and SMA connected to a custom-designed, fiber-optic diagnostic probe having three legs each comprising a fused silica fiber. It has touch-screen enabled graphic user interface (GUI) software (Fig. IV.9.2) to provide the necessary interface for the hardware control and data acquisition. It controls the spectrometer, its synchronization with the electrical signal generated by the IC-based hardware system and sequential switching of the respective excitation LEDs. One additional advantage of the software is that it has the ability to deliver online probabilistic diagnosis of the tissue site based on an instant analysis of the spectra.

Fig. IV.9.1: Tablet computer based, user-friendly cancer diagnostic system.

Fig. IV.9.2: A touch screen enabled GUI software for hardware control of the system, data acquisition and data analysis

IV.10. Development of a low cost tuberculosis (TB) screening and diagnostic device:

A compact and portable fluorescence imaging device (Fig. IV.10) was developed for rapid diagnosis of tuberculosis (TB). It acquires fluorescence images of mycobacterium tuberculi bacteria (Mtb) from a patient's sputum smeared on a microscope glass slide following its

staining with an appropriate fluorescent dye (Auramine O). The device uses a blue (460 nm) LED for fluorescence excitation. The excitation light is focused onto the dye-stained sputum smeared on the glass slide through a 40X microscope objective and the backscattered fluorescence signal from the bacteria is collected by the same lens and detected by a CCD camera. The fluorescence detection of Mtb is based on the fact that the mycolic acid on the cell wall of the bacteria binds with Auramine O dye to give green fluorescence when excited with blue light. A graphic user interface software developed enables hardware control of the device and automated counting of the Mtb bacteria. The important advantage of the device is its significantly low cost (~ 1 Lakh) as compared to the fluorescence microscope (costing over 50 Lakhs).

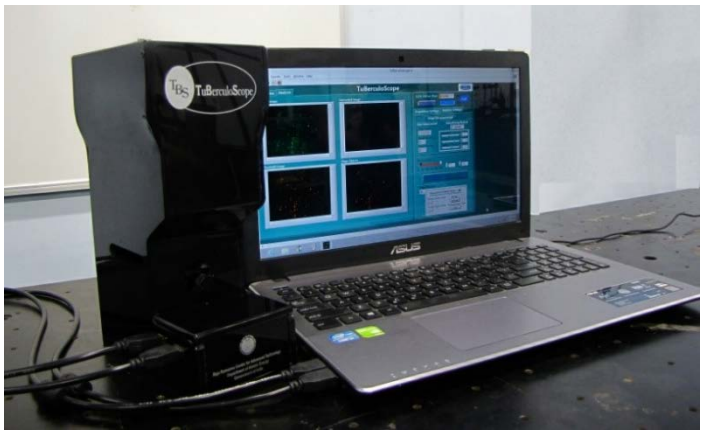

Fig. IV.10: Fluorescence imaging device for diagnosis of Tuberculosis.

IV.11. Development of a hand-held video microscope for non-invasive imaging of micro-vasculature and blood flow :

A compact hand-held video microscope (Fig. IV.11(a)) was developed for vivo imaging of micro-vasculature network and blood flow in human tissue. The blue light from a LED is collimated and plane polarized to illuminate the tissue. The light back scattered from the tissue is detected by a CMOS camera. Fig. IV.11(b) shows the orthogonal polarization image recorded with the help of the developed tool from the vasculature network of the inner lip in a human volunteer. The tool is expected to be helpful in monitoring the onset and progression of various diseases like diabetes, septic shock, tumor etc.

Fig. IV.11(a): Hand held orthogonal polarization spectral imaging setup for in-vivo imaging of micro-vasculature.

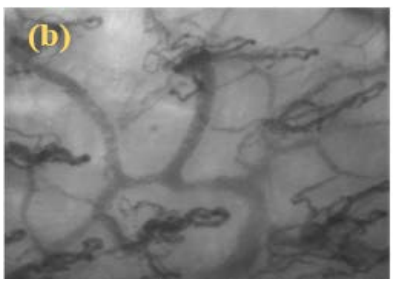

Fig. IV.11(b): Image of micro-vasculature in the inner lip of a human volunteer.

IV.12. Efficacy of in-house synthesized copper iodide complex of chlorin p6 for photodynamic treatment (PDT) of tumor in mice:

Studies were carried out on potential use of in-house synthesized copper iodide complex of chlorin p6 (ICp6Cu) for photodynamic treatment (PDT) of tumor in mice model. The tumors were allowed to grow ~10 - 15 mm in diameter after which the animals were used for the experiment. Photosensitizer was administered at a dose of 2.0 mg/kg body weight. To determine the tumor selectivity, at 4 h after injection the tumor and surrounding muscle tissues were removed, photosensitizer was extracted and its level in tissue extract was measured spectrofluorometrically. For PDT efficacy, at 4 hours after photosensitizer injection the tumor was superficially irradiated with red light (630 nm + 20 nm) at a dose of 100 J/cm^2. Results showed that metal complex accumulated efficiently in tumor and PDT with red light led to complete regression of tumor (Fig. IV.12).

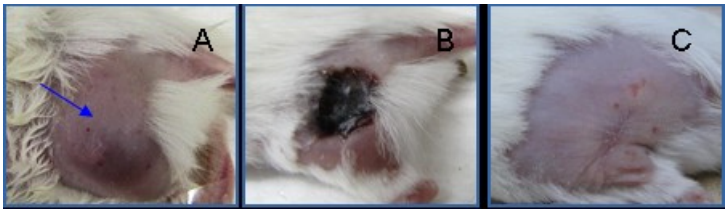

Fig.IV.12: Photographs of transplanted fibrosarcoma tumor on thigh region (arrow) of the mice that was subjected to PDT at 4 h after the administration of ICp6Cu (2.0 mg/kg). ***(A)*** *Before PDT,* ***(B)*** *24 h after PDT,* ***(C)*** *25 day after PDT.*

IV.13. Raman spectroscopy for detection of urea adulteration in packeted milk samples :

An inverse spatially-offset Raman spectroscopy (I-SORS) set up was developed (Fig. IV.13 (a)) for investigating the detection of urea adulteration in packeted milk samples.). Different samples of milk adulteration were prepared containing urea ranging from 10 to 500 mg/dl. I-SORS spectra (Fig. IV.13 (b)) were measured from the urea-mixed milk samples kept underneath a polythene packet. A partial least square (PLS) regression based chemometric algorithm was able to detect urea mixed in milk samples with an accuracy of >90 %. The results of this work indicate that the combination of inverse spatially offset Raman spectroscopy and chemometrics could be a promising tool for quantification of urea adulteration in packeted milk samples.

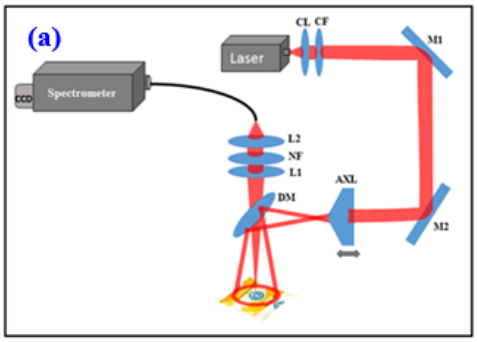

Fig.IV.13(a):Schematic of the inverse spatially offset Raman spectroscopy set-up.

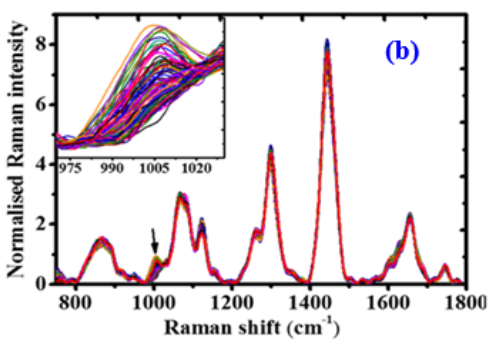

Fig. IV.13(b): Raman spectra of ten batches of milk samples adulterated with urea.

IV.14. Cold atom research :

An atom-chip with improved thickness of gold wires (from 100 nm to ~2 μm) was fabricated on Si-substrate (size 25 mm x 25 mm x 700 μm) and tested to enhance the current carrying capacity (up to ~1.0 A) of the wires on the chip for better magnetic trapping of atoms. The fabricated atom chip wires were characterized by flowing current through the wires and measuring their resistance at different values of current. The measured variation in resistance of a Z-shaped wire with time for different values of dc current is shown in Fig. IV.14.1. The results show that chip can sustain the required current of 1.0 A for the magnetic trapping of atoms near the chip surface.

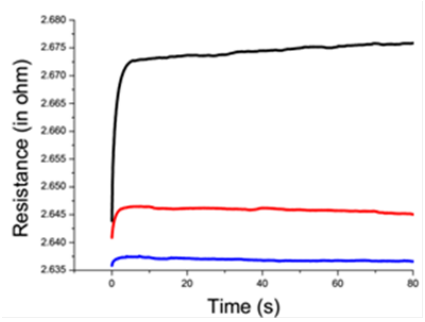

Fig. IV.14.1: Variation in the resistance of a Z-shaped wire on the chip with time for different values of current 0.3 A (blue curve), 0.5 A (red curve) and 1.0 A (black) respectively.

A dual-isotope magneto optical trap (MOT) for generation of cold fermionic (^{83}Kr)-bosonic (^{84}Kr) mixture of krypton atoms in metastable state has been successfully made operational for the first time. This cold fermionic-bosonic mixture of metastable Krypton (Kr) atoms is useful for studying the cold collision physics of krypton atom in metastable state. Simultaneous cooling and trapping of metastable ^{83}Kr (^{83}Kr*) and metastable ^{84}Kr (^{84}Kr*) atoms has been achieved by assembling a dual-isotope MOT, which can laser cool and trap both the isotopes ^{83}Kr* and ^{84}Kr* of krypton at the same spatial position. In these overlapping clouds of ^{83}Kr* and ^{84}Kr* atoms in the MOT, nearly 1 x 10^5 atoms of each isotope at temperature of ~ 400 μK and ~ 360 μK, for ^{83}Kr* and ^{84}Kr* respectively, have been trapped.

An optical lattice formed by structured laser beams after overlap of Gaussian and Bessel beams has been formed and a laser cooled atom cloud of ^{87}Rb atoms has been trapped in the lattice (Fig. IV.14.2). A double magneto-optical trap (MOT) setup for cooling and Bose-Einstein condensation of of ^{87}Rb atoms has been used in these experiments. The setup consists of a vapor chamber MOT (VC-MOT) at pressure ~2 x 10^{-8} Torr (with Rb-vapor) and an ultra-high vacuum chamber (UHV-MOT) at pressure of ~3x10^{-11} Torr. The cold atoms collected in VC-MOT were ejected from it by using a red-detuned push beam to load the UHV-MOT. The structured beams is formed in the vertical direction by creating interference of a Gaussian laser beam and a Bessel beam. The beams were kept red-detuned by ~ 25 GHz from the D_2 line transition of ^{87}Rb atom.

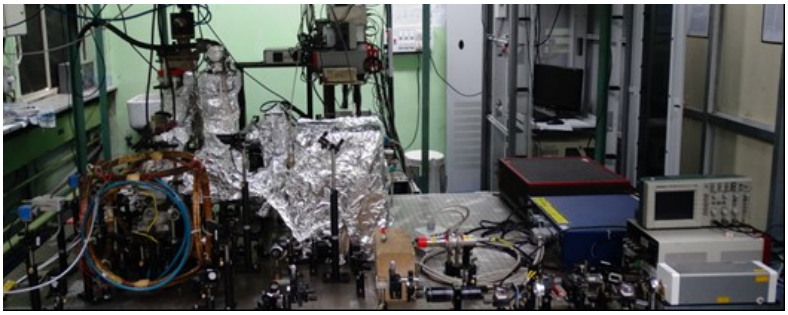

Fig. IV.14.2: Experimental setup to generate structured optical lattice.

Probe transmission through a Rb vapour cell has been controlled using a strong coupling beam in either travelling wave or standing wave configuration. This study can find applications in the optical switching devices which are useful for optical communication networks.

V. MATERIALS SCIENCE :

Several groups at RRCAT are carrying out research to study materials of potential technological interest, design, develop new materials, and develop prototype device structures. The main activities carried out this year are described below.

V.1. Special materials :

V.1.1. Demonstration of vortex–glass transformation within the surface superconducting state of the β-phase Mo1-xRex alloys :

The temperature dependence of electrical resistivity *ρ(T)* and heat capacity *C(T)* of the $Mo_{1-x}Re_x$ (x = 0.20, 0.25) refractory alloy superconductors were studied in different magnetic fields (Fig.V.1.1). In the presence of applied magnetic field, the electrical resistivity of these alloys goes to zero at a temperature well above the bulk superconducting transition temperature obtained with the help of heat capacity measurements in the same magnetic field. Analysis of the results indicates the presence of a surface superconducting state in these alloys, where the flux lines are pinned in the surface sheath of the superconductor. Experimental evidence in support of the surface mixed-state state or ‘Kulik vortex-state’ and the occurrence of a vortex–liquid to vortex–glass transition within this surface sheath was obtained.

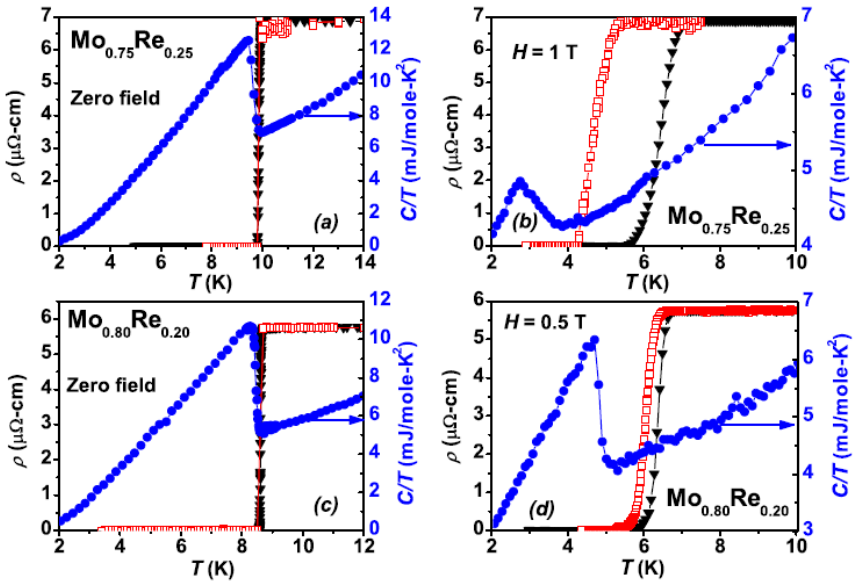

Fig.V.1.1: Temperature dependence of electrical resistivity and heat capacity in zero magnetic field (Panels (a) and (c)) and in the presence of 1 T and 0.5 T magnetic fields (Panels (b) and (d)) across the superconducting transition. In all the panels, the blue dots represent the heat capacity measured in different fields, the black solid triangles represent the electrical resistivity measured before coating the samples with Cu or Ag, and the red open squares represent the electrical resistivity measured after applying these metal coatings.

V.1.2. Demonstration of magneto electric coupling in nanocomposites:

$BiFeO_3$ (BFO)/(0.65Pb($Mg_{1/3}Nb_{2/3}$)O_3-0.35$PbTiO_3$)(PMN-PT) is an excellent ferroelectric material with high piezoelectric constant (d_{33} > 2500pC/N). Incorporation of nano BFO in highly insulating and piezoelectric PMN-PT improves the ferroelectric as well as magnetic properties of BFO due to interface interactions. In multiferroic composites, one can take advantage of electric field poling to achieve a higher piezoelectric coefficient and consequently a stronger ME coupling. BFO/PMN-PT bulk and nano-composites were fabricated and enhancement of ferroelectric, ferromagnetic properties and magneto electric coupling at room temperature were demonstrated. Scanning electron microscopy shows that $BiFeO_3$ and PMN-PT phase makes solid solution in bulk composites while asymmetric grain growth was observed in nano composites. The observed electric field poling induced magnetization exchange biasing makes this composite a possible candidate for spintronics and sensor applications.

V.1.3. Development of a magneto-photoluminescence and magneto-surface photo-voltage setup for quasi-simultaneous measurements :

A compact experimental assembly has been designed and fabricated for quasi-simultaneous measurement of magneto-photoluminescence and magneto-surface photo-voltage spectrum (Fig.V.1.3.1). The sample is kept inside a Dewar of thermostat surrounded by liquid helium chamber with helical shaped NbTi superconducting magnet, that produces magnetic field up to 8T. An indium tin oxide coated semi-transparent conducting glass plate is kept on the surface

of the sample and is exposed to fibre coupled laser light for PL measurements. PL signal is detected by a spectrometer. In case of SPV measurement, the same spectrometer is used to monochromatize the broad spectra from a quartz tungsten halogen lamp, and coupled to the optical fiber. The surface photo-voltage generated in the sample is then picked up by the ITO coated top electrode. The new experimental assembly is found to be beneficial for gaining a complete information on the dynamics of thermally excited charge carriers and the magnetic field driven charge carrier confinement on the radiative recombination efficiency of semiconductor quantum structures. The setup is specifically being used to study AlGaAs/GaAs and GaAs/InGaAs QW samples which are used for the development of laser diode arrays. A typical magneto-PL and magneto-SPV spectra of a GaAs/AlGaAs multi QW sample is shown in Fig.V.1.3.2. The spectra is recorded at 100K under 8 Tesla magnetic field. The facility is being utilized to study the effect of temperature and magnetic field on the radiative and non-radiative recombination processes in semiconductor quantum structures.

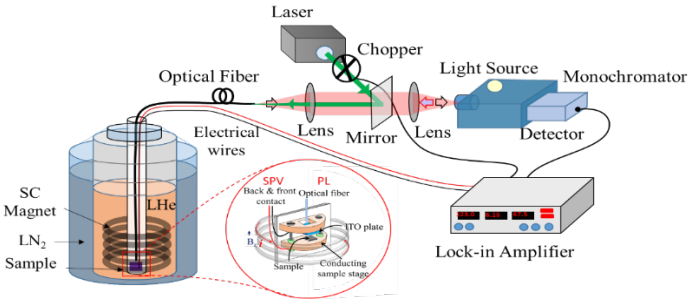

Fig. V.1.3.1: Schematic diagram of quasi-simultaneous magneto-photoluminescence and magneto-surface photo-voltage spectrum measurement setup.

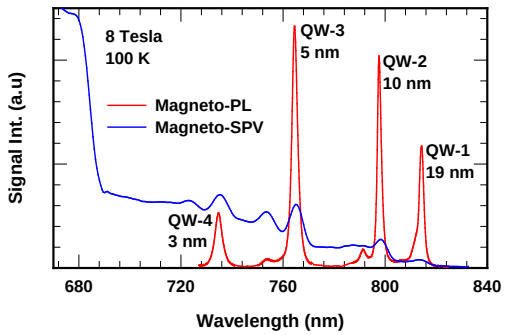

Fig. V.1.3.2 Quasi-simultaneous magneto-PL and magneto-SPV spectra of a GaAs/AlGaAs multi quantum well sample.

V.1.4. Femtosecond laser induced photoluminescence enhancement of quantum dots:

Increasing emission efficiency of quantum dots is important for several optoelectronic applications like LEDs, quantum dot lasers and bio-markers. We have demonstrated a photoluminescence (PL) enhancement process that depends on the heat generated by the femtosecond laser pulses in TGA-capped CdTe quantum dots dispersed in water. The average power densities required are in order of few W/cm2 and the time required is few tens of minutes. We find that in this process of enhancement the irradiation does not cause any significant shift in the PL and exciton absorption peaks (Fig.V.1.4). It has been shown that for a given power

density the rate of enhancement of PL is directly proportional to the absorption coefficient of the sample indicating that the heat generated by the laser exposure plays a strong role in enhancement of PL. This technique is useful for improving the PL from quantum dots as it is fast, causes no size change and the irradiated quantum dots are stable.

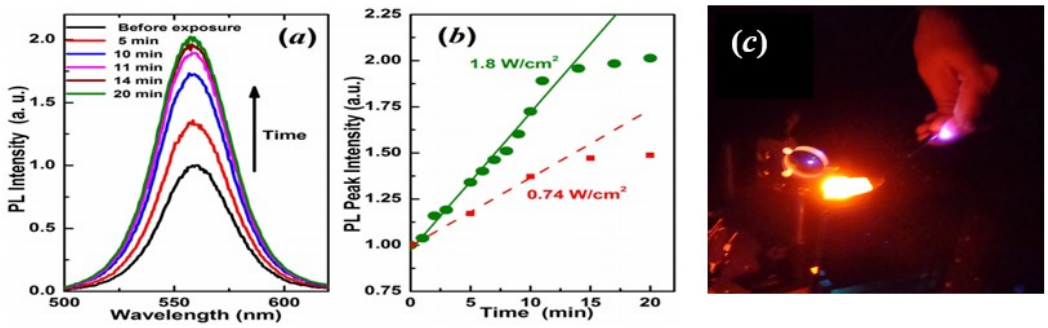

*Fig. V.1.4: The changes in the PL spectrum of CdTe quantum dots in water during irradiation by 400 nm femtosecond pulses at an average power density of 1.8 W/cm^2. **(a)** PL spectrum at few representative irradiation times, **(b)** the dependence of PL peak strength on irradiation time at two different average power density: 1.8 W/cm^2 (green dots) and ~0.9 W/cm^2 (red squares). The lines are linear fit to the data before 12 min. **(c)** Photograph of PL emission from quantum dots embedded in polymer.*

V.1.5. Growth and spectroscopic studies on nanomaterials :

To obtain measurable Raman spectroscopy signal in nanostructures, surface enhanced Raman scattering (SERS) can be employed using rough/nanostructure metal surfaces. The Langmuir Blodegtt technique is employed in TiO_2 nanostructures. Simulation studies on effect of temperature were carried out for predicting surface modification of InAs nanowire (NW) using laser irradiation. The surface modification was monitored by Raman spectroscopy. One dimensional nanostructures such as nanowires and nanobelts have attracted much attention due to their novel physical properties and technological applications in optoelectronic devices. Cadmium sulphide (CdS) is an important II-VI optoelectronic material finding applications for the light emitting diodes and photo-voltaic devices. In order to realize CdS nanostructure based devices, it is important to grow good crystalline quality one dimensional nanostructures, using relatively inexpensive method.

V.1.6. Theory and computational activities:

From first-principles calculations, we predict Co_2PtGa to possess low inherent crystalline brittleness as well as the high melting, martensite transition and Curie temperature; all of these well above the room temperature-which render it a promising material for application as a high temperature magnetic shape memory alloy.

Using density functional theory based calculations, we establish the implicit and important presence of RKKY interaction in Heusler alloys which are likely to exhibit magnetic shape memory effect.

V.2. Development of prototype device structures :

V.2.1. Demonstration of high speed resistive switching (switching times~ ns) in Au/NiO/Pt devices for fast and low power non-volatile data storage applications :

Au/NiO/Pt devices of ~200 μm diameter were synthesized through pulsed laser deposition and DC sputtering. The device displayed clear unipolar RS events between two stable states of high and low resistance (~ 12 kΩ and 48 Ω, respectively) with non-overlapping set and reset voltages (1.3-1.8 V and ~0.5-0.8 V, respectively). Ultra-fast resistive switching with write and erase time ~ tens of ns (about 1000 times faster than existing flash memory) has been demonstrated in Au/NiO/Pt devices at low switching voltages $\leqslant$ 3V. The device may find potential applications towards development of upcoming memory technology for non-volatile data storage applications.

V.2.2. Development of plasmonic gold nanoparticles based sensing technique for mercury detection (<100 ppb) in aqueous solution :

Detection of carcinogenic heavy metal ions (such as Hg, Pb, As) present in water due to natural or artificial processes, is important to maintain the pollutant free drinking water and aquatic ecosystem. Plasmonic gold nanoparticles were grown using laser ablation and wet chemical methods in citrate aqueous solutions. These were capped with thiol ligands to decrease their inter-particle separation and induce plasmon coupling. With this aggregation Hg^{2+} ions in aqueous samples was detected with concentrations of about 50 ppb. Typical colorimetric changes of the gold nanoaprticles with decreasing the Hg^{2+}ion concentration is shown in Fig.V.2.2. Plasmonic gold nanoparticles can be effectively utilised as real time and cost effective sensor by monitoring their colour (plasmon resonance wavelength) change with Hg^{2+} concentration.

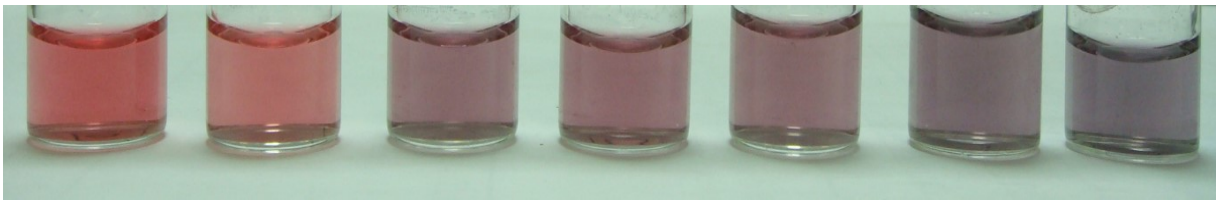

Fig.V.2.2.: Typical colorimetric changes of the gold nanoaprticles with decreasing the Hg^{2+} ion concentration from left: 30 μM, 3 μM, 300nM, 30 nM, 10 nm, 1 nM and without Hg^{2+}.

V.2.3. Development of InAsP/InP multiple quantum well based IR detectors:

Schottky junction based InAsP/InP multiple quantum well (QW) photodetectors have been fabricated and tested for infrared detector applications (Fig V.2.3). In this Au-Ge/Ni/Au metallic contacts were deposited on n^+InP substrate to form Ohmic contacts. Schottky

contacts were made of gold (Au) and Au wires were used to make the final electrical connection from both types of contacts. The measured spectral response of the fabricated detector show peak responsivity of 9 mA/W at around 1 μm wavelength.

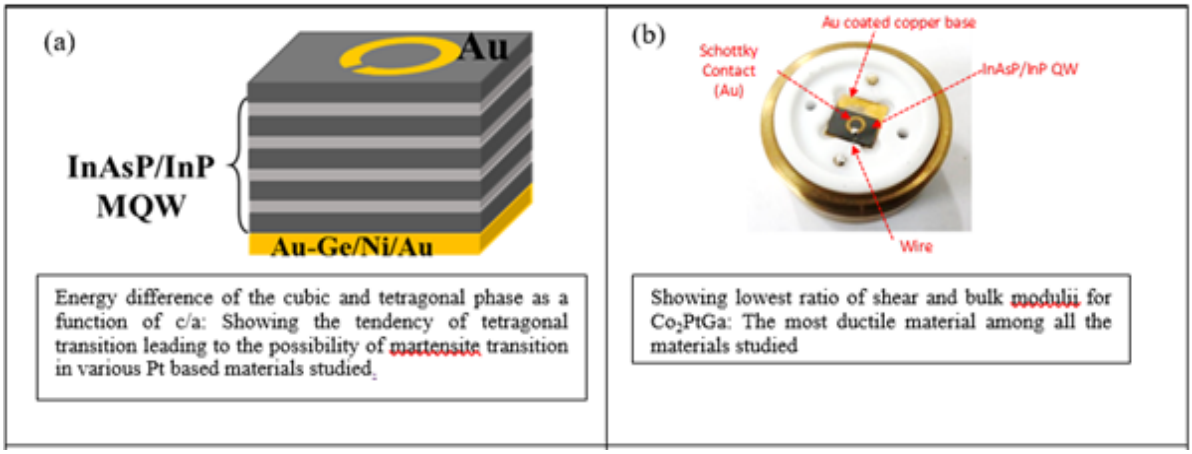

Fig. V.2.3: Schematic of InGaAs / GaAs QW recorded using the indigenously developed QW detectors.

V.2.4. Rare earth doped strontium barium niobate (SBN) single crystals for pyro-electricity based laser energy meter application :

Lead-free strontium barium niobate (SBN) is gaining considerable interest as pyroelectricity based infrared detector material due to its high pyroelectric coefficient. Undoped as well as Gd and Ce doped (0.125 & 0.25 mol % for both) $Sr_{0.61}Ba_{0.39}Nb_2O_6$ single crystals of ~6 mm diameter and 15 - 20 mm length were grown by the optical floating zone technique. Significant improvement in the detection sensitivity for pulsed Nd:YAG laser output (1064 nm, 7 ns) was observed in Gd doped SBN (~29 V/J) in comparison to undoped SBN (14 V/J).

V.2.5. Pt-Ti doped carbon aerogel catalyst for hydrogen isotope exchange:

Platinum carbon aerogel with partial substitution by titanium (Pt/Ti-CA) for cost effectiveness was synthesized and tested for the H/D isotope exchange in experimental hydrogen-water test column. The 25% Pt substituted by Ti [Pt / Ti (75:25)-CA] catalyst was evaluated. Isotope exchange efficiency and volume transfer rate of 83% and 0.3 m^3 (STP) $s^{-1}m^{-3}$ respectively were observed. The values are comparable to the performance of the Pt-CA catalyst tested under similar test conditions.

V.2.6. Transparent ceramic for x-ray imaging :

Cerium doped yttrium aluminum garnet (Ce:YAG) is a known scintillator used for the detection of ionizing radiation and medical radiographic imaging. Cerium (Ce) doped transparent YAG ceramic was developed in-house and tested for x-ray imaging on x-ray lithography beam line (BL-07) of Indus-2 (Fig. V.2.6.1). The x-ray beam passing through the object is absorbed/transmitted differently from the different part of the object. The

varying intensity falling on the ceramic sample produces visible image of the object due to scintillation effect. The image produced on ceramic scintillator was captured using a visible CCD camera. With this sample a spatial resolution of 15-20 micron has been achieved. Radiographic images of dead houseflies and black-ant as recorded on transparent Ce:YAG ceramic (Fig.V.2.6.2).

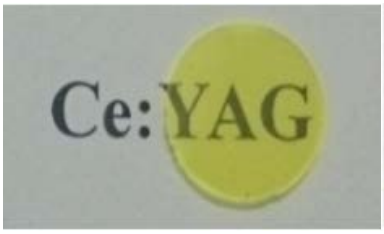

Fig. V.2.6.1: In-house developed transparent Ce:YAG ceramic.

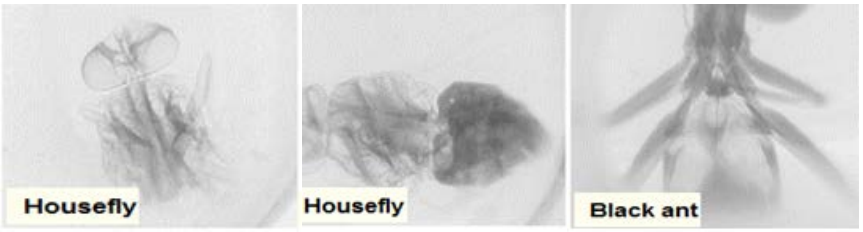

Fig. V.2.6.2: Radiographic images of dead houseflies and black-ant as recorded on transparent Ce:YAG ceramic.

V.2.7. Titanium thin film coating on Ceramic sample :

Magnetron sputtering system was used for the titanium coating on inner surfaces of DN 100 CF (Stainless steel) circular chamber (Fig. V.2.7.1). Co-centric probe technique was used to measure the coating thickness. The measured thickness was found to be ~0.8 to 0.9 µm. The coating was analyzed for its composite of various elements using SEM EDAX (Fig. V.2.7.2). It was found that Titanium-92.97%, Al-1.7%, Si-4.27%, Mg-1.07%**.** Optimization studies are in progress for coating on kicker ceramic chambers of Indus-2.

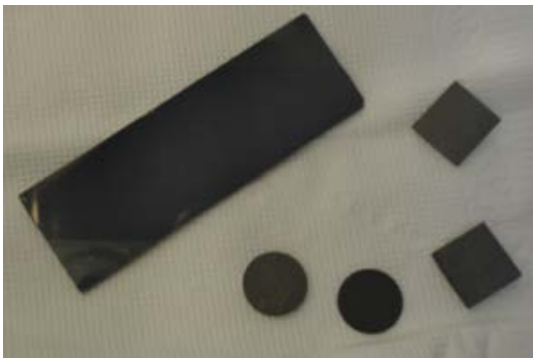

Fig..2.7.1: Titanium coated substrates.

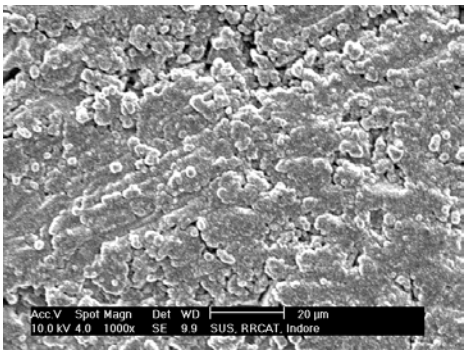

Fig V.2.7.2: SEM Image of Titanium film.

VI. INTERNATIONAL COLLABORATION :

VI.1. Development and installation of pulsed solid state power amplifier (SSPA) under DAE-CERN collaboration:

A solid state amplifier has been developed and installed at CERN, Geneva for energizing sub-harmonic, bunching system of the compact linear collider (CLIC) drive beam injector (Fig. VI.1.1). The amplifier provides up to 20 kW of peak power with pulse width of 140.3 µs and repetition rate of 50 Hz (Fig. VI.1.2). Amplifier features a 3 dB bandwidth of 58 MHz at centre frequency 499.75 MHz and gain of 59 dB at peak power. The amplifier has pulse to pulse phase and amplitude stability of better than 1° and 0.1 dB, respectively.

Fig.VI.1.1 : 20 kW Solid state power amplifier.

Fig.VI.1.2: Output Power of the SSPA.

VII. INFRASTRUCTURE :

VII.1. Computing Infrastructure :

VII.1.1. e-Governance : Various workflow based software applications have been developed and deployed on RRCAT Infonet (RRCAT information portal) which include:
e-Logbook for Indus beamlines, portal for personnel radiation dose monitoring, medical centre information management system, digital signature certificates (DSC) enabled applications for CL/Sp.CL and leave applications, workflow based software for online stores requisition with DSC based approval for issue of common stock items from IRSU, workflow based work requisition and approval software for online requisition for jobs to be fabricated in workshops, software for recording 'Out Duty' details of employees with e-approval by Head of Divisions / Independent Sections integrated with attendance details of individual employees.

VII.1.2. The data centre has been upgraded to accommodate 200 kVA of server load, distributed in 32 number of racks, with each rack of 42U size, capable of bearing 1200 Kgs of

physical server loads (Fig VII.1.2). Very Early Smoke Detection Apparatus (VESDA) and Novec 1230 (FK-5-1-12 agent) gas based fire suppression systems have also been integrated in the data centre. Video surveillance and biometric access control setup has also been integrated inside the data centre.

Fig. VII.1.2: Layout of the commissioned Data Centre.

VII.1.3. A new electronic messaging/mailing setup with enhanced user email data storage has been commissioned for in-house usage by ~2000 engineers / scientists / scholars / administrative staff working at RRCAT, Indore.

VII.1.4. A web based monitoring system has been designed, developed and commissioned to visualize the state of electric fence surrounding the RRCAT campus. Thereby empowering security personnel to monitor perimeter level intrusions and take necessary action well in time.

VII.1.5. Photograph and signature capture and upload setup has been developed for ID card preparation of employees using advanced RISC machines (ARM).

VII.2. Civil infrastructure :

VII.2.1. Construction of several new laboratory buildings has been completed.

Fig. VII.2.1.1: Ion exchange building.

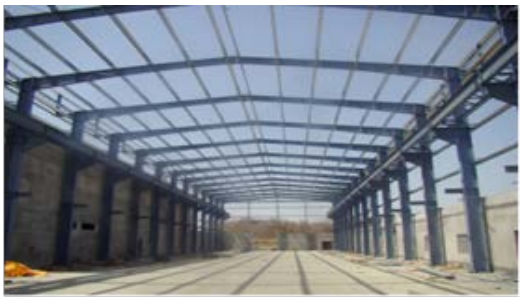

Fig. VII.2.1.2: PEB - Cryo module engineering lab.

Fig. VII.2.1.3: Support building for clean room of SCRF laboratory.

Fig. VII.2.1.4: CISF 'A' Type Quarters : 40 Nos

VII.2.2. Green initiatives: Implementation of regular vermi-composting activity to treat horticulture waste using earthworms has been completed. Landscaping has been done around the Sukhniwas lake. A new solar fountain has been installed and commissioned.

Fig. VII.2.2.1: Solar powered fountain.

Fig. VII.2.2.2: Vermi culture shed.

HUMAN RESOURCE DEVELOPMENT :

VIII.1. Human resources development activities:

Human resources development activities at RRCAT contribute in a significant way towards development of quality scientific and technical manpower in the country. Trainee scientific officers (TSOs) are imparted one year training in physics, electrical and electronics disciplines, which also serves as one year course work towards the successful completion of M.Tech. and Ph.D. degrees of HBNI, Mumbai. In the 17th batch, 4 TSOs have completed the one year orientation course in the field of Accelerators and Lasers and have been placed in various units of DAE. 3 TSOs who passed out previously from various BARC training schools and joined RRCAT as SO/C have been awarded M.Tech. degree. The number of Ph.D. scholars who have completed the one year pre-doctoral course are 6 and currently 4 Ph.D. scholars are undergoing the course work. During 2016-17, 10 scholars have been awarded Ph.D. degree by HBNI. RRCAT also provides the opportunity to M.Tech. /M.Sc. students of various universities and engineering colleges to carry out their one year/six months project work towards the partial fulfilment of their degrees. This year, a total of 110 students from various universities/ institutions completed their M.Tech. project work at RRCAT.

VIII. OUTREACH ACTIVITIES :

IX.1. Certificate Course: Every year, RRCAT conducts an eight week "Orientation Course on Accelerators, Laser and related Science and Technologies". The third edition OCAL-17 was conducted during 22 May - 14 July, 2017. In all, 40 post-graduate students (M.Sc., M.Tech., M.E.) from 16 states successfully completed the course which comprised lectures, invited talks, hands-on experiments, visits to RRCAT laboratories, students' seminar and an industrial visit. The course is aimed at motivating the bright young students in the country to take up their career in science and technology in general, and accelerators and lasers in particular.

Fig.IX.1.1. Shri G. Kalyanakrishnan, CE, NFC, Hyderabad speaking at the inaugural function of OCAL-17

Fig .IX.1.2. Shri S. K. Sharma, CMD NPCIL, distributing certificates in the concluding function of OCAL-17

IX.2. Participation in exhibitions: Under the outreach programme, RRCAT participated in four national exhibitions. These include (1) the "Pride of India" exhibition organized as part of 104th National Science Congress during January 3-7,2017 at Sri Venkateswara University, Tirupati; (2) Bhopal Vigyan Mela (BVM)-2017 held during March 3-6, 2017 at BHEL, Dussehra ground, Bhopal where the RRCAT Pavilion won the 2nd position amongst 120 exhibitors; (3) "Mega Science and Technology Expo" organized as part of India International Science Festival 2017 during October 13 -17, 2017 at Anna University, Chennai; (4) NUiCONE 2017 (exhibition on Green Technology and Innovations) at Nirma University, Gandhinagar by Institute of Plasma Research, Gandhinagar, organized during November 23-25, 2017.

IX.3. National Science Day Celebration: RRCAT celebrated National Science Day on 25th and 26th February, 2017 by holding an open house for school students, teachers, family members of staff members and invitees from public. A number of scientific exhibits were set up at different laboratories to explain the scientific and technical activities of RRCAT and to demonstrate a few concepts in basic sciences. About 1400 students and teachers of 105 schools from Indore and nearby places visited the exhibits. A special feature this year was the participation of deaf and mute students for which special arrangements were made using interpreters. A "Make in India Gallery" was set up to showcase recent important scientific achievements and in-house technology developments carried out at RRCAT.

IX. RTI DETAILS :

The number of RTI applications received and disposed of during January to December 2017 are given below.

Months	**No. of RTI applications received**	**No. of applications disposed of**
January	16	09
February	05	12
March	17	13
April	17	12
May	12	17
June	17	11
July	08	17
August	24	21
September	21	14
October	08	15
November	16	09
December	10	06
Total	**171**	**156**